INVESTIGATION OF FUEL CYCLE FOR A SUB-CRITICAL FUSION-FISSION HYBRID BREEDER REACTOR

A Thesis
Presented to
The Academic Faculty

by

Christopher L. Stewart

In Partial Fulfillment
of the Requirements for the Degree
Masters of Science in Nuclear Engineering in the
School of Mechanical Engineering

Georgia Institute of Technology
December 2013

INVESTIGATION OF FUEL CYCLE FOR A SUB-CRITICAL FUSION-FISSION HYBRID BREEDER REACTOR

Approved by:

Dr. Weston Stacey, Advisor
School of Mechanical Engineering
Georgia Institute of Technology

Dr. Bojan Petrovic
School of Mechanical Engineering
Georgia Institute of Technology

Dr. Anna Erickson
School of Mechanical Engineering
Georgia Institute of Technology

Date Approved: October 01, 2013

ACKNOWLEDGEMENTS

I would like to thank my parents for providing me with a loving and supportive environment which cultivated my love for science and the drive to pursue it; my advisor, Professor Stacey for his insight, guidance, and reassurance throughout my introduction to the discipline of nuclear engineering; Professor Petrovic who helped refine my understanding of reactor physics; the past and present members of the Georgia Tech Fast Reactor Research Group and Fusion Research Center for being there to bounce ideas off of and making work a fun place to go; the NEUP program for financially supporting me during my research; and lastly Tara Mostowy for her encouragement, companionship, and love which uplifts my spirits daily.

TABLE OF CONTENTS

LIST OF TABLES

LIST OF FIGURES

LIST OF SYMBOLS

MW_{th}	10^6 Watts (Thermal)
U	Uranium
Pu	Plutonium
Zr	Zirconium
D	Deuterium
T	Tritium
cm	10^{-2} Meters
MW	10^6 Watts
He	Helium
n	Neutron
MeV	10^6 Electron Volts
Li	Lithium
Si	Silicon
O	Oxygen
mm	10^{-3} Meters
ºC	Degree Celsius
Nb	Niobium
at%	Atomic %
w%	Weight %
Fs	Fissium
eV	Electron Volt

Na	Sodium
Fe	Iron
Cr	Chromium
Ni	Nickel
keV	10^3 Electron Volts
P_{fus}	Fusion Power
P_{fis}	Fission Power
E_{fus}	Energy Released per Fusion Event
E_{fis}	Energy Released per Fission Event
k_{mult}	Neutron Source Multiplication Factor
k_{eff}	Neutron Multiplication Factor
ν	Average # Neutrons Released per Fission
Σ_j^i	Macroscopic Cross-Section of Species *i* for reaction *j*
$\phi(\mathbf{r},t)$	Neutron Flux at Position **r** at Time *t*
$S(\mathbf{r},t)$	Neutron Source at Position **r** at Time *t*
$\rho_{subcrit}$	Reactivity Margin to Criticality
β	Delayed Neutron Yield
kg	10^3 Grams
yr	Year
W	Watt
g	Gram

LIST OF ABBREVIATIONS

SABR	Subcritical Advanced Burner Reactor
IFR	Integral Fast Reactor
PRISM	Power Reactor Innovative Small Module
ITER	International Thermonuclear Experimental Reactor
SABrR	Subcritical Advanced Breeder Reactor
ERANOS	European Reactor Analysis Optimized Calculation System
LWR	Light Water Reactor
FFH	Fusion-Fission Hybrid
TBR	Tritium Breeding Ratio
FBR	Fissile Breeding Ratio
ODS	Oxide-Dispersion Strengthened
MA	Mechanically Alloyed
DPA	Displacements per Atom
EBR	Experimental Breeder Reactor
BoC	Beginning of Cycle
ECCO	European Cell Code
Hex3D	Hexagonal, 3-Dimensional
JEF	Joint Evaluated Fission and Fusion
EoC	End of Cycle
efpy	Effective Full-power Years
DU	Depleted Uranium

S-PRISM	Super-PRISM
TRU	Transuranics
OD	Outer Diameter
%TD	% Theoretical Density

SUMMARY

The SABR fusion-fission hybrid concept for a fast burner reactor, which combines the IFR-PRISM fast reactor technology and the ITER tokamak physics and fusion technology, is adapted for a fusion-fission hybrid reactor, designated SABrR. SABrR is a sodium-cooled 3000 MW_{th} reactor fueled with U-Pu-10Zr. For the chosen fuel and core geometry, two configurations of neutron reflector and tritium breeding structures are investigated: one which emphasizes a high tritium production rate and the other which emphasizes a high fissile production rate. Neutronics calculations are performed using the ERANOS 2.0 code package, which was developed in order to model the Phenix and SuperPhenix reactors. Both configurations are capable of producing fissile breeding ratios of about 1.3 while producing enough tritium to remain tritium-self-sufficient throughout the burnup cycle; in addition, the major factors which limit metal fuel residence time, fuel burnup and radiation damage to the cladding material, are modest.

CHAPTER 1

INTRODUCTION

Closing the nuclear fuel cycle is an important step in advancing the prospect of nuclear energy in both the near and far term. The once-through cycle largely employed today uses a very small percentage of the potential energy content of natural uranium and produces high-level waste for which we have yet to implement a long-term solution. A solution to the overall fuel cycle problem would have the dual benefits of extending the uranium resources of Earth by a factor of 10-100 over the once-through cycle and of greatly reducing the volume, decay heat, and longevity of repository-bound waste. Various fast reactor technologies and designs have been developed with the intent of closing the front end[1,2] (breeder reactors), the back end[3-5] (burner reactors), or both[6-8].

Breeder reactors take advantage of the high neutron-per-fission yield of fissile isotopes, particularly ^{239}Pu, in fast neutron spectra to supply extra neutrons beyond those necessary to sustain the fission chain reaction. These excess neutrons are captured in fertile material such that more fissile material is produced than was consumed. Burner reactors leverage a fast neutron spectrum to transmute, preferably by fission, transuranic isotopes which remain in the spent fuel discharged from thermal reactors. These transuranics, which constitute a substantial fraction[4] (tens of percent) of burner reactor fuel, would otherwise be sent directly to a geological repository and dominate the long-term radiotoxicity and decay heat of the used nuclear fuel[9,10]. Some reactor designs[6-8] incorporate the aspects of both breeders and burners. They are intended to operate in an integrated fuel cycle, mixing their own discharged fuel with used fuel from other reactors and depleted uranium to form the next fuel loading. One of the most mature of these integrated reactor concepts is the Integral Fast Reactor (IFR)[6,7,11]; many of its design

decisions and material choices reflect the very hard neutron spectrum its fuel cycle requires.

A Subcritical Advanced Burner Reactor (SABR) concept is being developed at the Georgia Institute of Technology which addresses the waste problem[12,13]. SABR is a sodium-cooled, 3000 MW_{th} annular fast reactor consisting of 4 assembly rings surrounding a toroidal plasma. The fission core operates in the subcritical regime; the plasma supplies an external neutron source via the D-T fusion reaction. The fuel pins of SABR are loaded with transuranics processed from used fuel from LWR's which is fissioned to a high at% burnup. Neutrons leaking from the fission core are captured in surrounding Tritium breeding blankets in order to produce fuel for the fusion reaction. Because of the subcritical operation, SABR is postulated to be able to be fueled with 100% transuranic fuel discharge from LWR's, as contrasted with the tens of percent envisioned for critical reactors[4]. Fuel cycle calculations[14,15] indicate that SABR could consume transuranics at triple the rate that an LWR of the same power output produces them – a future reactor fleet might then produce 75% of its electricity in LWR's and 25% in SABR's and send no transuranics, other than losses from reprocessing, to repositories. SABR is based on existing technologies developed for the IFR and on ITER physics and technology, and could be deployed by mid-century.

Because the plasma and technology performance required for an economical fusion power plant significantly exceeds that which will be demonstrated in ITER, developing fusion-fission hybrid (FFH) reactors with ITER-level plasma and technology requirements in parallel with the further plasma and technology development needed for pure fusion power would allow for substantial accumulation of power reactor operating experience with tokamaks prior to the introduction of pure fusion power plants into reactor fleets[13]. In the near term, these fission-fusion hybrids (FFH's) would likely be devoted to burning actinides, while in the longer term, using them for fissile production becomes more desirable as easy-to-extract ^{235}U becomes depleted. The SABR studies

indicate the efficacy of the FFH in the burner role. An important question then arises: could a similar hybrid reactor make a useful contribution as a breeder?

Moir et al[16,17] have explored a fission-fusion hybrid breeder in some depth, exploring economic scenarios and materials choices with respect to different fertile isotopes and LWR support ratios. Those studies focused on a tandem mirror fusion device with substantially different geometry than SABR. Nevertheless, the important considerations are the same as for a tokamak-geometry fast breeder. The primary challenge when designing an effective breeder is the neutron economy: of the neutrons released from each fission, somewhat less than one neutron on average must go toward sustaining the chain reaction, a fraction are captured parasitically in fissile material and structural materials, a fraction leak out of the reactor, and the remainder are available for absorption in fertile material to breed fissile material.

The purpose of this study is to investigate the technical feasibility of adopting the basic SABR configuration and fusion physics and technology to the purpose of fissile production. Instead of the transuranic fuel used in the SABR burner reactor, the fuel pins for the breeder reactor SABrR contain U-Pu-Zr and U-Zr metal fuel. The primary difference in neutronics design challenge between the burner and breeder SABRs revolves around the neutron economy. Whereas in the burner reactor only the total fission rate and the Tritium Breeding Ratio (TBR) are important, in the breeder reactor, the TBR, the Fissile Breeding Ratio (FBR), and the fission rate are important. Previous calculations indicate that a TBR > 1.15 must be achieved in order to provide for Tritium self-sufficiency of the fusion neutron source, and a FBR of significantly greater than unity must be achieved to provide fissile material for other reactors. The challenge of keeping a sufficiently high TBR in SABrR is exacerbated by the presence of U-Zr fissile-breeding blankets between the annular fission core and the surrounding tritium-breeding blanket, which significantly reduces the neutron flux incident on the tritium breeding blankets in the breeder relative to the burner. With this in mind, two somewhat different

configurations of the tritium blanket and reflector structures were considered – one which maximizes the TBR and one which maximizes the FBR.

CHAPTER 2

SABrR DESIGN CONCEPT

SABrR Design Overview

The top-level configuration of the SABR burner concept is shown in Figure 2.1, and a more detailed R-Z cross section is shown in Figure 2.2.

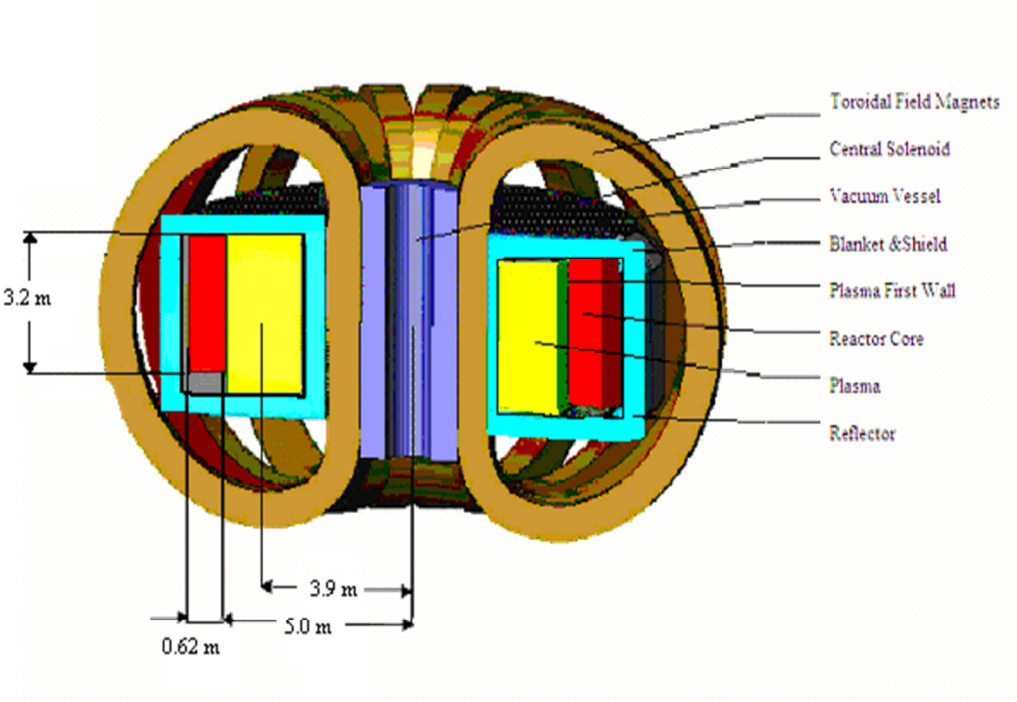

Figure 2.1: SABR Configuration

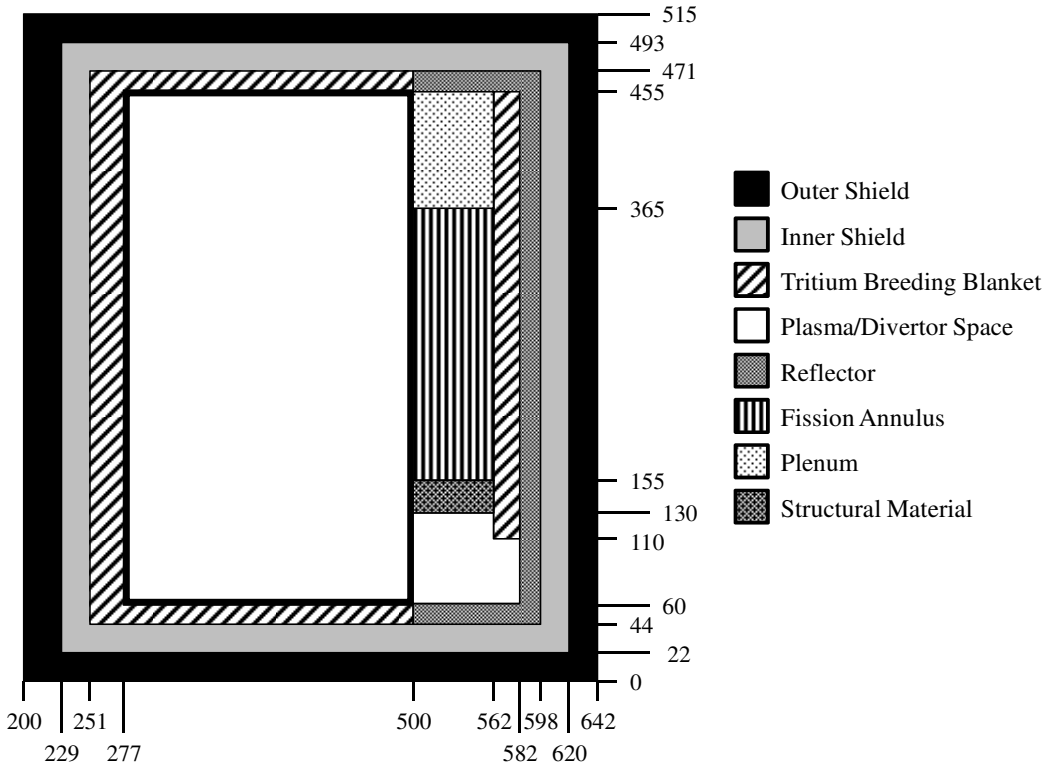

Figure 2.2: R-Z Cross Section of SABR (dimensions in cm)

The entirety of the fusion and fission systems resides within the superconducting toroidal magnets of the tokamak. The inner edge of the annular fission core lies at the outer edge of the tokamak plasma chamber wall. Surrounding the plasma chamber and fission core annulus are first the tritium breeding blankets and then stainless steel reflectors. Finally, these are enveloped by multi-layer shields which reduce the fast neutron and gamma fluences to the superconducting magnets, giving them a lifetime of at least 30 full-power years.

Fusion Neutron Source

The fusion neutron source is provided by a tokamak based on ITER physics and fusion technology and is capable of 500 MW of fusion power. Deuterium and tritium in the plasma undergo the reaction ${}_1^2D + {}_1^3T \rightarrow {}_2^4He + {}_0^1n$. The He nucleus will deposit most of its energy, about 3.5 MeV, into the plasma. However, the neutron, carrying 14.1 MeV,

will stream directly out of the plasma since it has no charge and is therefore not bound by the magnetic fields confining the plasma. This neutron, possessing energy several times that of the average fission neutron, is extremely well-suited to sustain a subcritical fission reaction: not only is the fission-to-capture ratio for heavy metal nuclides higher at such high energies, the neutron also has energy well in excess of the threshold fission reactions in the even-neutron isotopes, of which ^{238}U, ^{240}Pu, and ^{242}Pu are of primary importance. Furthermore, (n,2n) and (n,3n) reactions contribute substantially to neutron production via the fusion source due to the increase of these cross sections at high neutron energy.

It is not difficult to obtain half of the fuel for the D-T fusion reaction – deuterium, present in about 1 of every 10,000 water molecules, is relatively easy to recover. Tritium, however, has a half-life of 12.32 years and must therefore be produced. To do so, tritium breeding blankets composed of Lithium Orthosilicate, Li_4SiO_4, are placed around the plasma chamber and fission annulus. Lithium occurs naturally in two isotopes; 7% is ^{6}Li and 93% is ^{7}Li. Tritium is therefore produced by the reactions

$$ {}^{6}_{3}Li + {}^{1}_{0}n \rightarrow {}^{3}_{1}T + {}^{4}_{2}He \tag{1} $$

$$ {}^{7}_{3}Li + {}^{1}_{0}n \rightarrow {}^{3}_{1}T + {}^{4}_{2}He + {}^{1}_{0}n \tag{2} $$

The latter reaction is endothermic with a threshold energy of E_n = 2.466 MeV, whereas the former is exothermic. This, combined with the high absorption cross section of ^{6}Li for neutrons at thermal energies, causes the ^{6}Li reaction to be far more effective at tritium production despite its much lower isotopic content. The Li in SABrR's tritium breeding blankets is enriched to 93% ^{6}Li by weight to increase the tritium production rate.

Annular Fast Reactor

Each SABrR fuel assembly (Figure 2.3) is a hexagonal duct measuring 15.5 cm across-flats[12] made of ODS MA957, a ferritic oxide dispersion strengthened steel which is estimated to withstand up to 200 DPA.

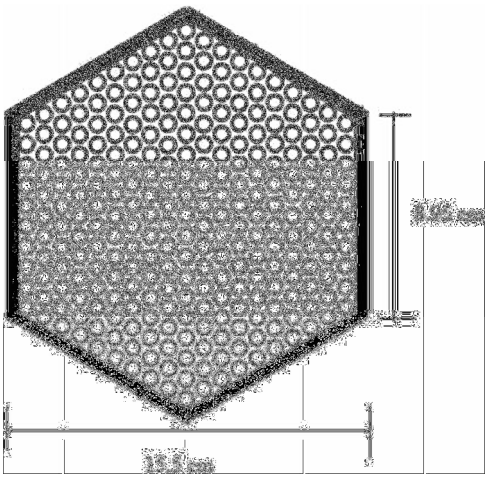

Figure 2.3: SABrR Fuel Assembly

The duct is filled with 10 rings of fuel pins on a hexagonal lattice, for a total of 271 pins per assembly. The pins are separated by a wire wrap at a pitch of 8.9 mm. The fuel pins (Figures 2.4a and 2.4b) are based on the pins developed in the Integral Fast Reactor initiative for Super-PRISM[18]. The cladding, like the duct, is ODS MA957. ODS MA957 was developed as a low-swelling ferritic steel for fast reactor cladding; at low-temperature irradiation (T < 355 °C) the ductile-to-brittle transformation temperature shifts upward significantly, causing embrittlement as a failure mode at relatively low accumulated radiation damage[19,20]. For this reason, the lowest cladding temperature in SABrR is ~380 °C, and is located at the lower edge of the lower axial blanket, where the fast neutron fluence is significantly below average; similarly, the region of maximum fast fluence (at the core midplane) has cladding temperatures well in excess of 400 °C. Around the cladding is a $LiNbO_3$ sheath which provides electrical insulation in order to prevent a large magnetohydrodynamic pressure drop in the liquid metal coolant.

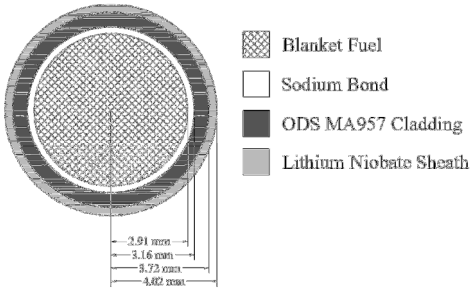

Figure 2.4a: SABrR Fuel Pin

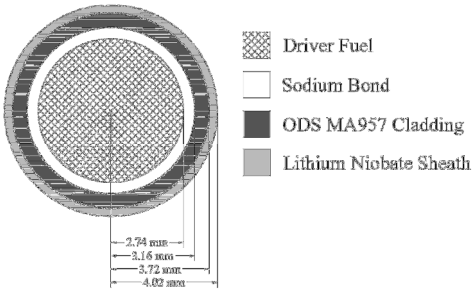

Figure 2.4b: SABrR Blanket Pin

The fission core fuel height is 200 cm, but this is axially expanded to 210 cm in the computational model to account for thermal and irradiation-induced axial swelling which occurs at very low burnup[21-23]. The densities are correspondingly adjusted downward in order to keep the fuel mass constant. An R-Z cross section of the fuel zones in the fission annulus is shown in Figure 2.5. The driver fuel is located in the axially-centered 150 cm of the 2nd and 3rd assembly rings. There are 30 cm axial blankets both below and above the driver fuel. Radial breeding blankets fill assembly rings 1 and 4.

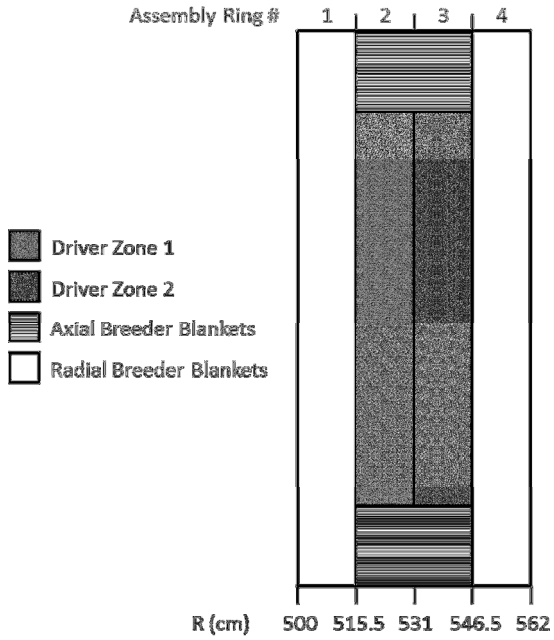

Figure 2.5: SABrR Fuel Loading

The driver fuel is a U-Pu-10Zr ternary alloy very similar to several of the pin compositions tested in EBR-II and the Fast Flux Test Facility[21,24]. The fuel slug has a smear density of 75% in order to allow for burnup-related swelling due to the production of gaseous fission products. These gases cause the fuel to become porous and swell radially until it contacts the cladding. At about 1 at% burnup, the porosity is high enough that the pores become interconnected and the fission gases are released to the plenum; further gaseous fission products which are produced do not contribute to further swelling, and thus high burnups are achievable[22,23]. In some of the test pins in EBR-II, burnups of almost 20 at% were demonstrated in several of the test pins without issue; these tests were ongoing when the reactor was shut down, so 20 at% can be considered a lower limit of the burnup potential of that fuel. The Plutonium vector of the driver fuel is given in Table 2.1; it was developed for high-burnup metal fuels[14]. The Plutonium enrichment in Driver Zone 2 (in the 3rd assembly ring) is 23.75 w%, slightly higher than in Driver Zone 1, at 22.36 w%, in order to flatten the radial power profile – it receives fewer fusion neutrons as it is farther away.

Table 2.1: BoC Plutonium Vector of Driver Fuel

Isotope	% (weight)
^{238}Pu	2.102
^{239}Pu	58.258
^{240}Pu	25.976
^{241}Pu	9.76
^{242}Pu	3.904

The radial blanket fuel is a U-10Zr alloy at 85% smear density; it is similar to the Mark-I fuel pins for EBR-II, except with 10% Zr by weight instead of 5% Fs (Fs is "Fissium", an alloying element meant to approximate metallic fission products which would accompany the heavy metals during pyrometallurgical reprocessing). The ^{235}U enrichment is 0.25% by weight. The 10% Zr was chosen because of its beneficial effect

on the fuel melting temperature and fuel-cladding-chemical-interactions. While the reduced Uranium concentration likely has a slightly negative effect on breeding, the plasma-side edge of the inner radial blanket receives the fusion neutrons most directly and thus has relatively high power for a fast reactor blanket; therefore the thermal considerations are of primary importance. For that same reason, the pin diameter and number of pins per assembly are kept the same as in the driver fuel rather than using the fewer, larger pins found in most blanket assembly designs. The Mark-II fuel pins were limited to 3 at% burnup in EBR-II due to burnup-induced swelling; these pins are similarly limited.

The axial blankets are the same composition as the radial blankets, but at 75% smear density to allow the fission gases from the driver fuel easy access to the plenum. Because of their lower smear density, the burnup limit of the axial blankets matches that of the driver fuel.

The breeding of fissile material occurs by neutron capture in fertile isotopes within the fission annulus. The primary fertile isotope is ^{238}U, which captures a neutron and then decays by beta emission twice before becoming fissile ^{239}Pu:

$$ {}^{238}_{92}U + {}^{1}_{0}n \rightarrow {}^{239}_{92}U^{*} \xrightarrow{\beta} {}^{239}_{93}Np \xrightarrow{\beta} {}^{239}_{94}Pu \tag{3} $$

The decay to ^{239}Np occurs with a half-life of 23 minutes, and the decay to ^{239}Pu has a half-life of 2.4 days – thus ^{239}Np reaches near-steady-state levels very shortly after the beginning of the fuel residence. There are two fertile isotopes of Pu as well: ^{238}Pu and ^{240}Pu. Each of these can capture a neutron to become ^{239}Pu and ^{241}Pu, respectively:

$$ {}^{238}_{94}Pu + {}^{1}_{0}n \rightarrow {}^{239}_{94}Pu \tag{4} $$

$$ {}^{240}_{94}Pu + {}^{1}_{0}n \rightarrow {}^{241}_{94}Pu \tag{5} $$

Because ^{238}U is the most common isotope of the three in the fresh driver fuel, most of the fissile production is through the first reaction, though all three substantially contribute. In the blanket assemblies, only ^{238}U is initially present, so nearly all fissile production there occurs via ^{239}Np.

CHAPTER 3

COMPUTATIONAL MODEL

Calculation Methodology

SABrR was modeled in ERANOS[25] (European Reactor ANalysis Optimized calculation System), a fast reactor code system developed in order to model the Phenix and SuperPhenix reactors. ERANOS employs the European Cell COde (ECCO) to collapse fine-group cross sections within each reactor cell to the broad groups used in core calculations. The core geometry can be described in R-Z cylindrical geometry or in Hex3D geometry; diffusion and transport flux solvers are available for both geometries. ERANOS also contains modules for post-processing of the flux data.

Cross-Section Processing

ECCO uses group-averaged infinite-dilution cross sections derived from JEF-2.2 data, available in fine (1968 groups), intermediate (175 or 172 groups), or broad (33 groups) energy structure, ranging from 20 MeV down to 0.1 eV. Sub-group data is also available to calculate resonance shielding effects. ECCO carries out some procedures which are specifically designed for fast reactors. Matrix generation for elastic slowing-down from light elements Na and O and intermediate elements Fe, Cr, and Ni, as well as inelastic scattering from fuel isotopes is done at the fine-group level, as these are the primary contributors to neutron slowing-down in fast reactors. Self-shielding is carried out in the narrow-resonance approximation in the 100-keV to 1-keV energy range. Finally, streaming effects are given a detailed geometrical treatment across the lattice of pins, as the mean free path of fast neutrons is on the order of the size of an assembly.

The cross sections for the driver fuel were calculated in four steps in ECCO. In the first step, a buckling search is performed on the driver assembly in heterogeneous

geometry in the broad energy structure. The P1 collision-probability method is used to solve the flux distribution in the assembly; the leakage from each region is treated using a non-leakage factor calculated using the Benoist formula for the diffusion coefficient. In the second step, the buckling found in step 1 is used on the heterogeneous geometry to calculate self-shielding in the heavy metals and important structural isotopes using the fine energy group libraries; the modified cross-sections are then condensed to 33 energy groups. In step 3, a buckling search is re-performed under the same parameters as in step 1, but this time with the 33-group cross sections calculated in step 2. The 4^{th} step homogenizes the fuel assembly and, using the cross sections from step 2 and the buckling from step 3, calculates the fundamental mode flux solution, and produces an output library containing the 33-group self-shielded cross sections and diffusion coefficients to be used in core calculations. The library also contains leakage flux data which can be used in the cell calculations of subcritical assemblies or structural components.

The cross sections for the blanket regions were calculated in three steps in ECCO. In the first step, a subcritical flux solution is calculated with the nearest driver leakage considered as an external source. The assembly is treated in heterogeneous geometry with the broad group cross section input library for all elements. The buckling is set as $\frac{5}{8}\left(\frac{\pi}{Cell\ Width}\right)^2$, and the diffusion coefficient and leakage are treated in the same manner as in the driver fuel. Step 2 calculates the self-shielding of the heavy metals and primary structural elements using the fine energy cross section library and condenses the modified cross sections to 33 groups similarly to the second step of the driver fuel calculations, but a factor of DB^2 is added to the total cross section in the self-shielding calculation. This factor effectively reduces the energy self-shielding to account for the fact that the incident neutrons from the external source have a spectrum which is only partially dependent on the resonances in the blanket materials. The third step homogenizes the blanket assembly and calculates the fundamental mode flux solution for the external

source and buckling defined in step 1 on the subcritical assembly; an output library for each blanket region is created.

The structural regions are handled similarly to the blanket regions, except that there is no fine group self-shielding step. The structure cells are described in homogeneous geometry and the self-shielding in broad energy groups is calculated with the DB^2 modification to the total cross sections. The buckling is defined as in the blanket case and the external source incident on the region is defined using the output library of the nearest blanket zone.

Core Calculations

SABrR is modeled in R-Z geometry for the core calculations; the materials filling each zone are the homogenized outputs calculated in ECCO. Each of the four assembly rings composing the fission core of the reactor is divided into multiple slices (Figure 3.1) in order to increase the detail on the burnup calculation and to more accurately represent the response to the neutron source as fissile material is bred into the blankets, some of which border the plasma. Each driver assembly region is split radially into two halves. The inner and outer radial blanket assemblies are divided into 4 radial slices each, and the upper and lower axial blankets are divided into 6 axial slices each.

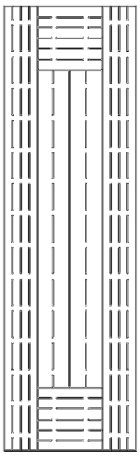

Figure 3.1: Fuel Zone Slices

The core calculations were carried out in BISTRO, the discrete ordinates module of ERANOS, using an S8 quadrature with 132 radial and 216 axial meshes and 33 energy groups. The fusion neutron source (E_n = 14.1 MeV) was represented as an isotropic source in the 1st energy group that was uniformly distributed throughout the entire volume of the plasma chamber. The fuel was depleted for 100 days in each burnup step in the EVOLUTION module before re-performing the core neutron flux calculations. The heavy metal mass and fission products from each fuel slice were homogenized within the slice at the end of each burnup step. The new composition was loaded into the corresponding slice, and new cross-sections were generated using ECCO that reflected the new composition of each zone – which was particularly important for the blanket regions.

At each burnup step the neutron source multiplication, k_{mult}, is calculated, and the neutron source strength is adjusted such that the fission annulus output is 3000 MW_{th}. The fusion power, P_{fus}, required to maintain a given fission power, P_{fis}, is determined by k_{mult}, the average number of neutrons released per fission, ν, the energy released per fusion, E_{fus}, and the energy released per fission, E_{fis}:

$$P_{fus} = P_{fis}\left(\frac{1-k_{mult}}{k_{mult}}\right)\nu\left(\frac{E_{fus}}{E_{fis}}\right) \tag{6}$$

It is important to note that k_{mult} differs from the more familiar k_{eff}. The TBR is also calculated at each step in order to determine if enough tritium is being produced to fuel sustained operation of the fusion neutron source. The TBR is defined as

$$\mathrm{TBR}(t) = \frac{\int_V \Sigma_c^{Li}\phi(\mathbf{r},t)\,dV}{\int_V \mathrm{S}(\mathbf{r},t)\,dV} \tag{7}$$

where S(**r**,*t*) is the fusion neutron source. This only accounts for production of tritium by ^{6}Li capture and thus is a conservative estimate of the TBR, as tritium produced in the threshold reaction in ^{7}Li is not counted in the ERANOS calculation. However, since the tritium breeding material is highly enriched in^{6}Li and the cross section for production via that route is much higher, the approximation should be quite close to the true tritium production rate.

The FBR is calculated as the instantaneous ratio of the production rate of fissile atoms to their destruction rate, whether through fission or parasitic capture.

$$\mathrm{FBR}(t) = \frac{\mathrm{P}(t)}{\mathrm{D}(t)} \tag{8}$$

The production rate is calculated by integrating the capture rates of the fertile isotopes over the reactor volume.

$$\mathrm{P}(t) = \int_V \left(\Sigma_c^{^{238}U}(\mathbf{r})\phi(\mathbf{r},t) + \Sigma_c^{^{238}Pu}(\mathbf{r})\phi(\mathbf{r},t) + \Sigma_c^{^{240}Pu}(\mathbf{r})\phi(\mathbf{r},t) \right) dV \tag{9}$$

Though ^{239}Np, rather than ^{238}U, is technically the precursor to ^{239}Pu, ^{239}Np exists in the reactor in a near-steady-state after its first few half-lives. Thus, by approximately day 20 of fuel residence time, the decay rate of ^{239}Np is equal to the capture rate of ^{238}U. The destruction rate is the volume-integrated absorption rate for all of the fissile isotopes. Only ^{235}U, ^{239}Pu, and ^{241}Pu exist in substantial amounts in the reactor, so other fissile isotopes are omitted from the summation.

$$\mathrm{D}(t) = \int_V \left(\Sigma_{abs}^{^{235}U}(\mathbf{r})\phi(\mathbf{r},t) + \Sigma_{abs}^{^{239}Pu}(\mathbf{r})\phi(\mathbf{r},t) + \Sigma_{abs}^{^{241}Pu}(\mathbf{r})\phi(\mathbf{r},t) \right) dV \tag{10}$$

Substituting these expressions for the production and destruction rates into (8), we have

$$\mathrm{FBR}(t)=\frac{\mathrm{P}(t)}{\mathrm{D}(t)}=\frac{\int_V\left(\Sigma_c^{^{238}U}(\mathbf{r})\phi(\mathbf{r},t)+\Sigma_c^{^{238}Pu}(\mathbf{r})\phi(\mathbf{r},t)+\Sigma_c^{^{240}Pu}(\mathbf{r})\phi(\mathbf{r},t)\right)dV}{\int_V\left(\Sigma_{abs}^{^{235}U}(\mathbf{r})\phi(\mathbf{r},t)+\Sigma_{abs}^{^{239}Pu}(\mathbf{r})\phi(\mathbf{r},t)+\Sigma_{abs}^{^{241}Pu}(\mathbf{r})\phi(\mathbf{r},t)\right)dV} \quad (11)$$

Design Constraints

There were 4 hard constraints placed on the reactor design which, if violated, were a termination point for that particular case. First, the TBR must not fall below 1.15. This value was chosen because tritium self-sufficiency is a requirement for sustained fusion operation and previous calculations indicate that this excess above unity allows for losses due to inefficiency in Tritium collection and for the radioactive decay of any Tritium in inventory throughout the operating and refueling cycles. Second, the radiation damage limit of the clad must not be exceeded. The damage limit of ODS MA957 steel in a fission spectrum is estimated at either 200 displacements per atom (DPA) or at an accumulated fast fluence of 4×10^{23} n/cm^2. Third, no blanket zone may surpass 3 at% burnup, as per the EBR-II Mark-II fuel pin tests. Fourth, no driver fuel may exceed 13.33 at% burnup – this is reduced from the 20 at% reached in the IFR pin tests because whereas most fast reactor fuel pins have a plenum-to-fuel volume ratio of unity, the SABrR pins have a ratio of only 2/3.

There were also soft constraints placed on each case, which were considered more as design guidelines. If a soft constraint is violated, the scenario may be continued if either the violation is temporary, or if a scenario is approaching the violation of a hard constraint. There were two soft constraints. First, k_{eff} should be significantly below 1 ($k_{eff} < 0.95$ was desired), such that $|\rho_{subcrit}| \gg \beta$, and the reactor is always very far from prompt critical. Second, the output of the fission core + blankets should be maintained at 3000 MW_{th} using a maximum of 500 MW of fusion power, the ITER design power level.

CHAPTER 4

GEOMETRIES SIMULATED

TBR Case

The configuration of reflector and tritium breeding blanket which emphasizes a high TBR is shown in relation to the fission core and plasma in Figure 4.1.

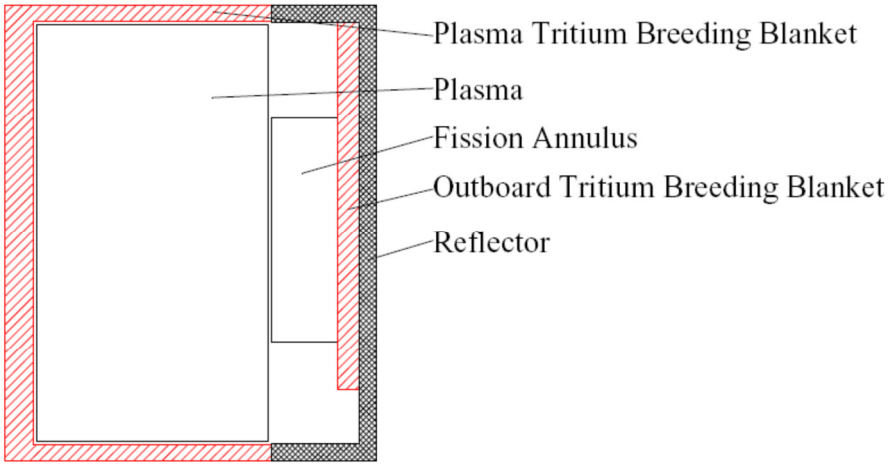

Figure 4.1: Configuration Favoring TBR (other reactor structures omitted)

Placing the outboard Tritium breeding blanket adjacent to the fission annulus results in a higher neutron capture rate in that blanket than if it were located radially outside the reflector. However, the increase in neutron capture comes at the expense of some of the fissile breeding in the outer radial fissile blanket, since neutron capture in the tritium breeding blanket competes with capture by the fertile isotopes.

FBR Case

The configuration of reflector and Tritium breeding blanket which emphasizes a high FBR is shown in relation to the plasma and fission core in Figure 4.2. The dimensions of the outboard reflector and tritium breeding blanket are the same as in the

TBR case, but with their positions switched. The goal of this geometry is to return more neutrons to the fission annulus than in the TBR case and to remove competing neutron capture from the outboard tritium breeding blanket.

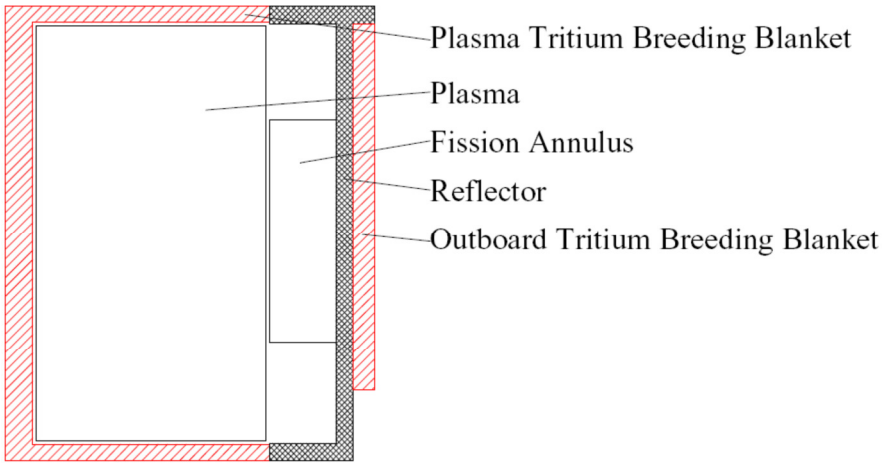

Figure 4.2: Configuration Favoring FBR (other reactor structures omitted)

Electrically Insulating Sheath Removed

A sensitivity study was performed on the FBR configuration in order to evaluate the effects of removing the $LiNbO_3$ insulating sheath from around each fuel pin. The motivation for the study stems from the need to compare SABrR with critical fast breeder reactors, which do not require an insulator since there are no strong magnetic fields present in those reactors inhibiting coolant flow. The lithium and oxygen in the insulator slow neutrons more in each collision than the sodium coolant which would normally occupy their space. While oxide-fueled reactors will have oxygen present in greater fractional quantities than SABrR, lithium is absent in even those cores, and represents a moderating element unique to SABrR. Though the insulating sheath is less dense than the cladding, it occupies 9.5% of the cross-sectional area within each fuel assembly, so its effect on the neutron spectrum is non-negligible.

The unsheathed driver and blanket pins are shown in Figures 4.3a and 4.3b. The reactor geometry is otherwise identical to the FBR configuration for the sensitivity study.

The duration of the scenario was kept the same as the FBR case in order to allow for a better comparison at the end of cycle.

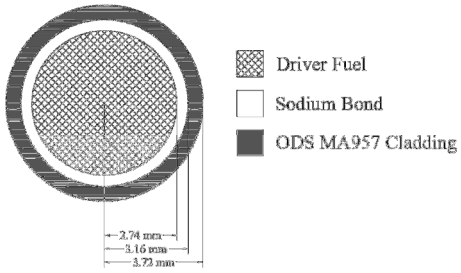

Figure 4.3a: Unsheathed SABrR Fuel Pin

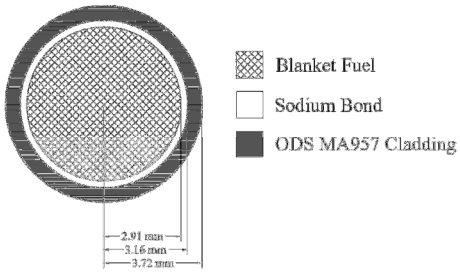

Figure 4.3b: Unsheathed SABrR Blanket Pin

Depleted Uranium Loading

A fourth case was examined in which the entire fission annulus was loaded with the depleted uranium of the fission blankets. All of the assemblies in all four rings in this case are identical to the radial breeding blankets in rings 1 and 4 of the other cases – the fuel is at 85% smear density. The 3 at% burnup limit corresponding to the radial blanket fuel applies to all of the fuel in this case. Because this case was unlikely to achieve 3000 MW_{th} fission power at the beginning of cycle using a 500 MW fusion neutron source, that constraint was lifted. Instead, the fusion power was kept at its maximum for the entire duration of the scenario or until the fission annulus became capable of 3000 MW_{th} output, at which point the fusion power was reduced accordingly. The geometry of the reflector and outboard tritium breeding blanket for this case is the same as the FBR case.

CHAPTER 5

RESULTS

Summary of Major Results

The major neutronic parameters of each of the TBR, FBR, and unsheathed cases are summarized in Table 5.1. Those parameters violating soft constraints are highlighted in yellow, and those which caused termination of their scenario are highlighted in red. The DU fuel loading was unable to obtain tritium self-sufficiency of the fusion system at any point during its fuel residence, and has been excluded from the summary for this reason. Its results are included in its section below.

Table 5.1: SABrR Neutronics Results

Quantity	TBR Case	FBR Case	Unsheathed Case
BoC k_{eff}	0.935	0.953	0.971
EoC k_{eff}	0.847	0.865	0.879
BoC k_{mult}	0.726	0.781	0.870
EoC k_{mult}	0.587	0.619	0.666
BoC P_{fus} (MW)	274	202	108
EoC P_{fus} (MW)	513	446	364
FBR (peak/EoC)	1.299/1.278	1.340/1.298	1.301/1.277
Fissile Gain (kg/yr)	208.4	253.7	212.4
Fuel Residence Time (yr)	6.3	7.12	7.12
TBR (minimum)	1.272	1.206	1.366
Peak DPA	112	124	134
Peak Fast Fluence (10^{23} n/cm^2)	2.79	3.12	3.38
Peak Blanket Burnup (at%)	2.95	2.98	2.43
Peak Driver Burnup (at%)	9.31	10.23	10.48

In general, k_{mult} was highly dependent on the k_{eff} of the fission annulus, so the negative burnup reactivity swing of all 3 cases required the fusion power to increase throughout the fuel residence time. This decrease was offset somewhat by production of

^{239}Pu in the plasma-adjacent blanket material, such that the increase slowed significantly after the initial few timesteps and increased by only a few MW per hundred days near the end of the burnup cycle. The burnup of the blanket material in the plasma-adjacent blanket ring was the limiting factor for the TBR and FBR cases; the unsheathed case was constrained to the same duration as the FBR case.

TBR Case

The k_{eff}, k_{mult}, and fusion power required to drive the fission annulus at 3000 MW_{th} are shown in Figure 5.1. Shortly before reaching 2000 days of fuel residence time, the fusion power required to maintain 3000 MW_{th} of fission power exceeds 500 MW. However, if the scenario is allowed to continue, the blanket fuel in the plasma-side edge of the inner radial blanket reaches 3 at% burnup soon after day 2300, with a required fusion power of 513 MW.

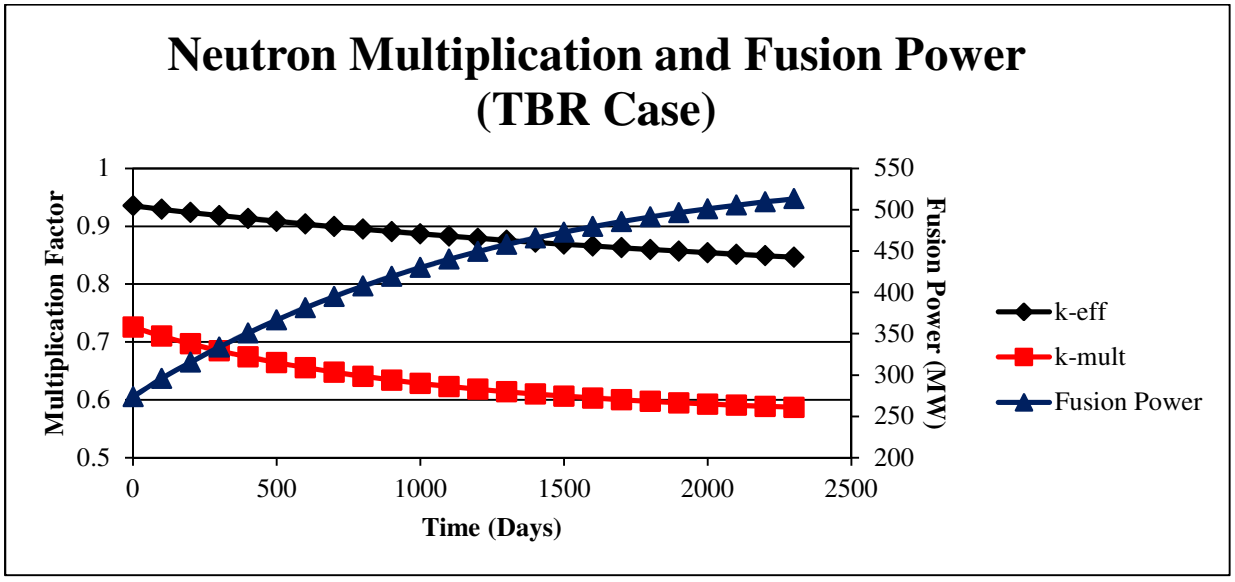

Figure 5.1: Neutron Multiplication Values and Fusion Power for TBR Case

The TBR as a function of time is shown in Figure 5.2. The TBR throughout the cycle is well in excess of the 1.15 necessary to produce fuel for the fusion reaction. The tritium production in the plasma-adjacent blankets tracks the source strength very closely

and these blankets on their own provide a TBR of approximately 1. The tritium production in the outboard blanket is nearly constant throughout the cycle.

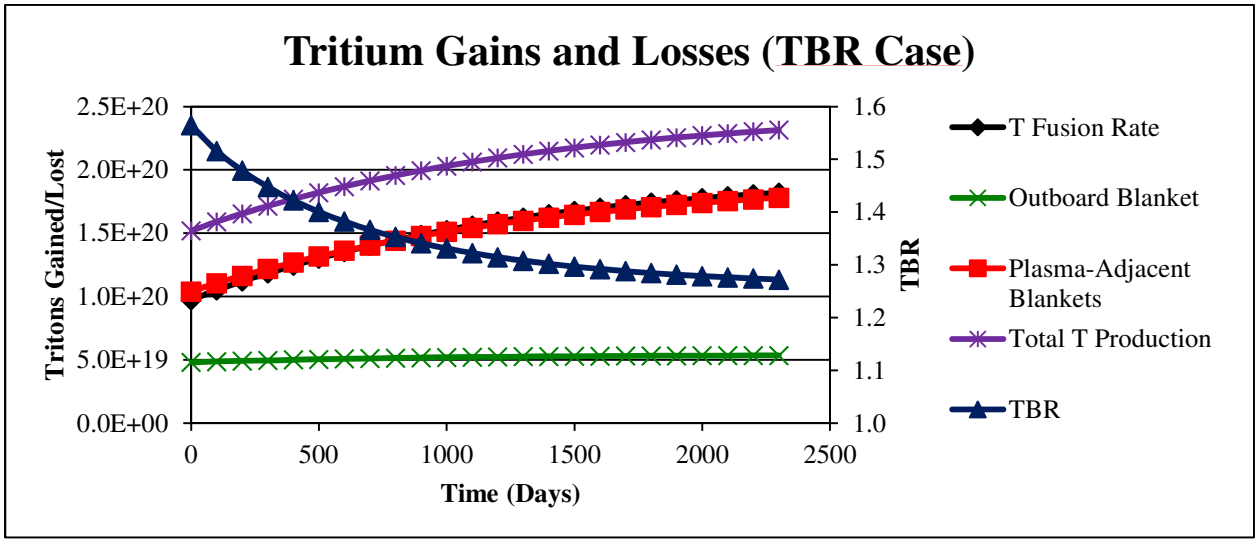

Figure 5.2: Tritium Breeding for the TBR Configuration

The net fissile gain (current – BoC) for each of the primary fissile isotopes (^{235}U, ^{239}Pu, and ^{241}Pu) is shown in Figure 5.3. ^{233}U has been omitted because it exists only in trace amounts in SABrR. The peak value of the FBR (1.299) occurs near day 1300 of fuel residence time, after which the FBR declines gradually to its end of cycle (EoC) value of 1.278. The average net fissile production rate for the TBR case is 208.4 kg/efpy (effective full-power year).

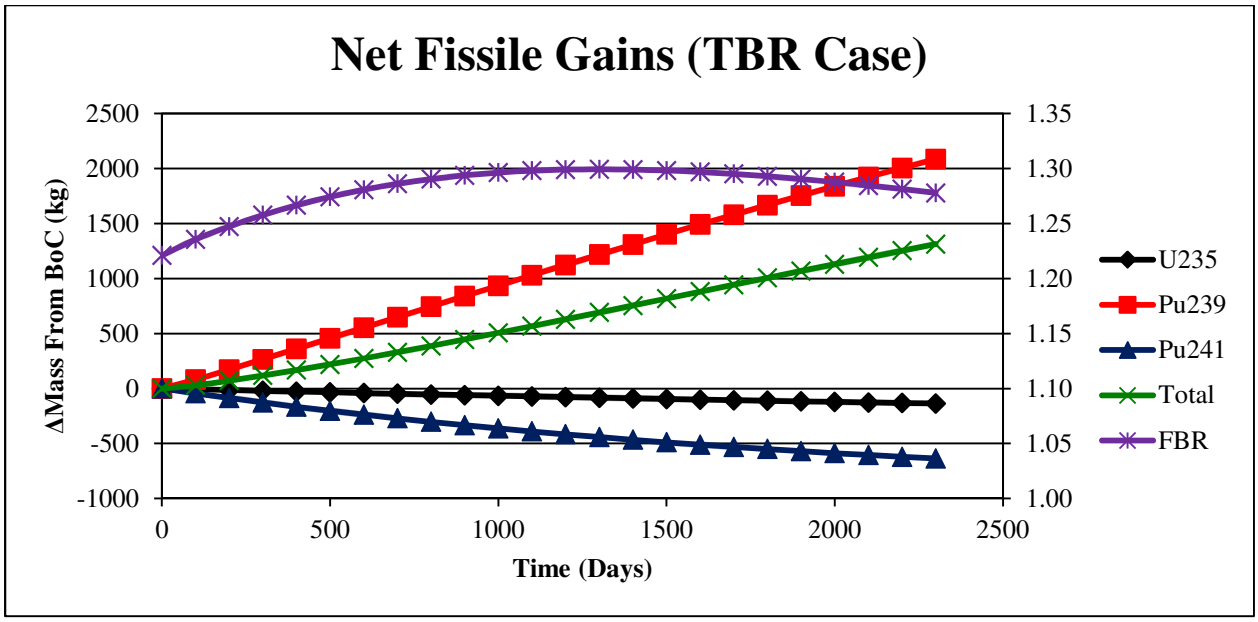

Figure 5.3: Fissile Breeding for the TBR Configuration

The maximum burnup in the driver fuel is 9.31 at%, well below its burnup limit of 13.33 at%. The maximum burnup in the blanket fuel is 2.95 at%, which occurs at day 2300 in the plasma-adjacent slice of the radial breeding blanket in ring 1 of the fission annulus.

The fast fluence ($E_n > 0.1$ MeV) and DPA accumulation in the cladding across the fission core midplane are shown in Figure 5.4 at various points throughout the fuel life. The EoC values are given at 2300 days of fuel residence time. The peak fast fluence at EoC is 2.79 x 10^{23} n/cm^2, and the peak DPA is 112. Both of these are significantly within their limits.

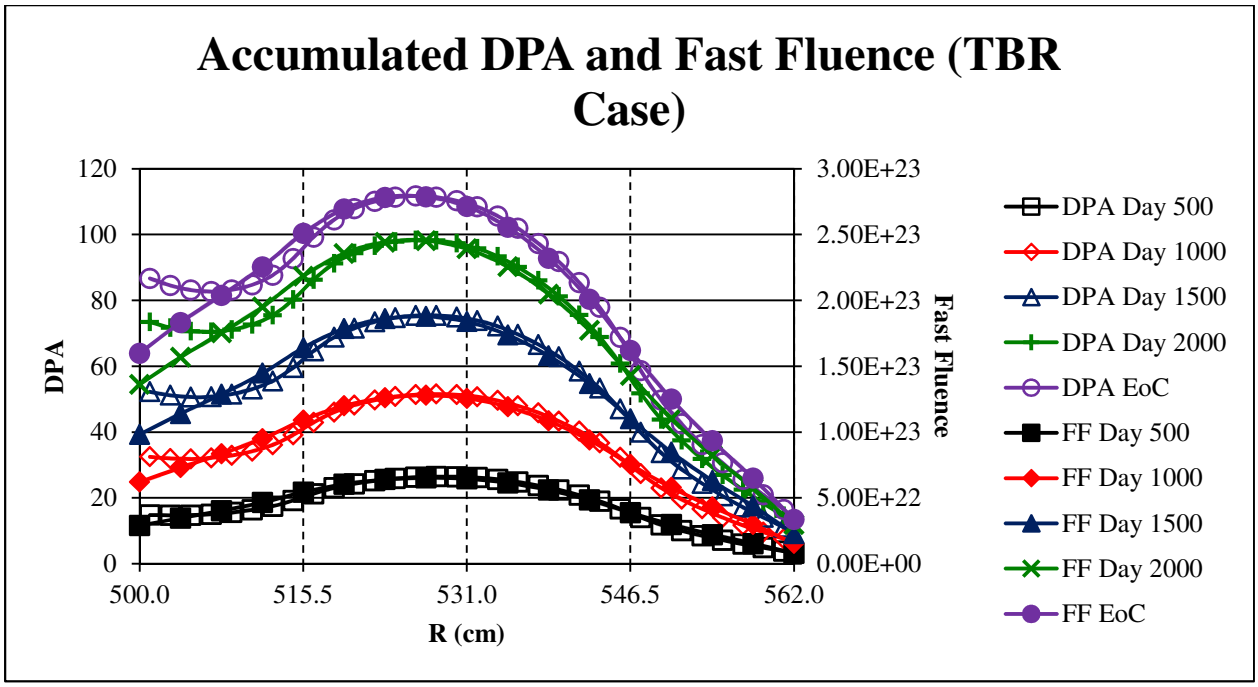

Figure 5.4: Radiation Damage for the TBR Configuration

FBR Case

The k_{eff}, k_{mult}, and fusion power required to drive 3000 MW_{th} in the FBR case are shown in Figure 5.5. The limiting factor for fuel residence time in this configuration is, as in the TBR case, the burnup limit of the plasma-edge blanket fuel being reached. However, because of the relatively lower fusion power throughout the entire residence time and the consequently lower contribution to the 3000 MW_{th} fission output from that zone, it took 2600 days to reach the 3 at% limit. Unlike in the TBR case, there is substantial margin to the maximum fusion power strength throughout the cycle.

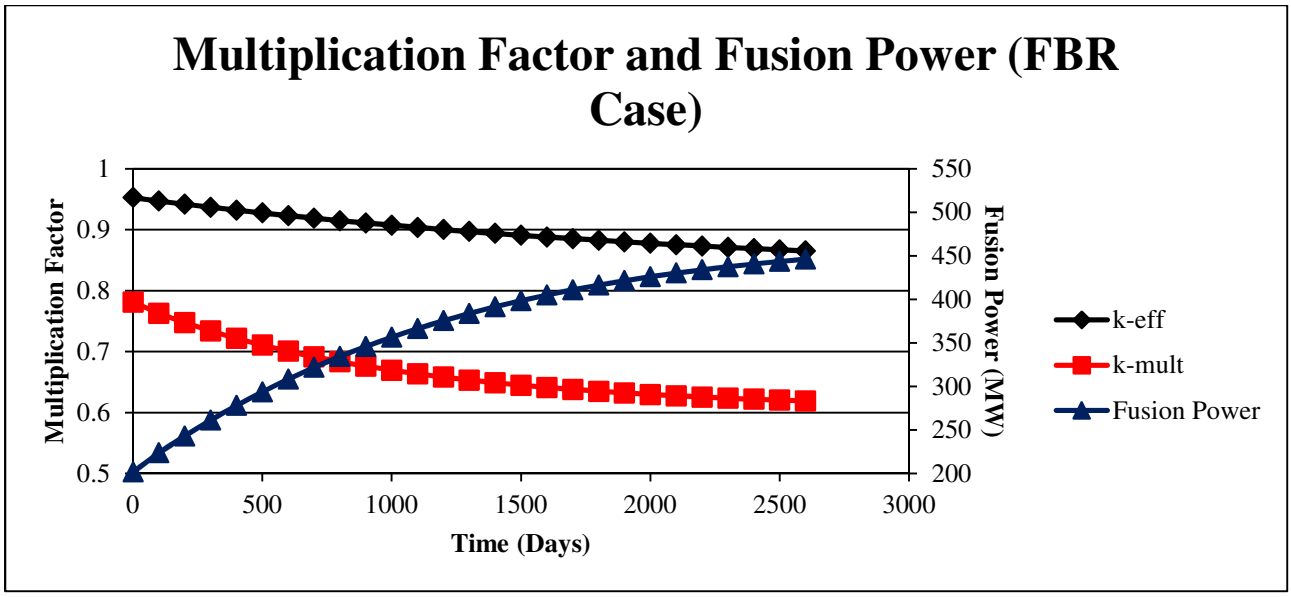

Figure 5.5: Multiplication Values and Fusion Power for FBR Case

The TBR as a function of time for the FBR case is shown in Figure 5.6. The TBR throughout the cycle exceeds 1.15, but with a smaller margin than for the TBR case, especially near EoC. Similar to the TBR case, tritium production in the plasma-adjacent blankets tracks the source strength very closely and exceeds the destruction rate slightly; the tritium production in the outboard blanket is nearly constant throughout the cycle.

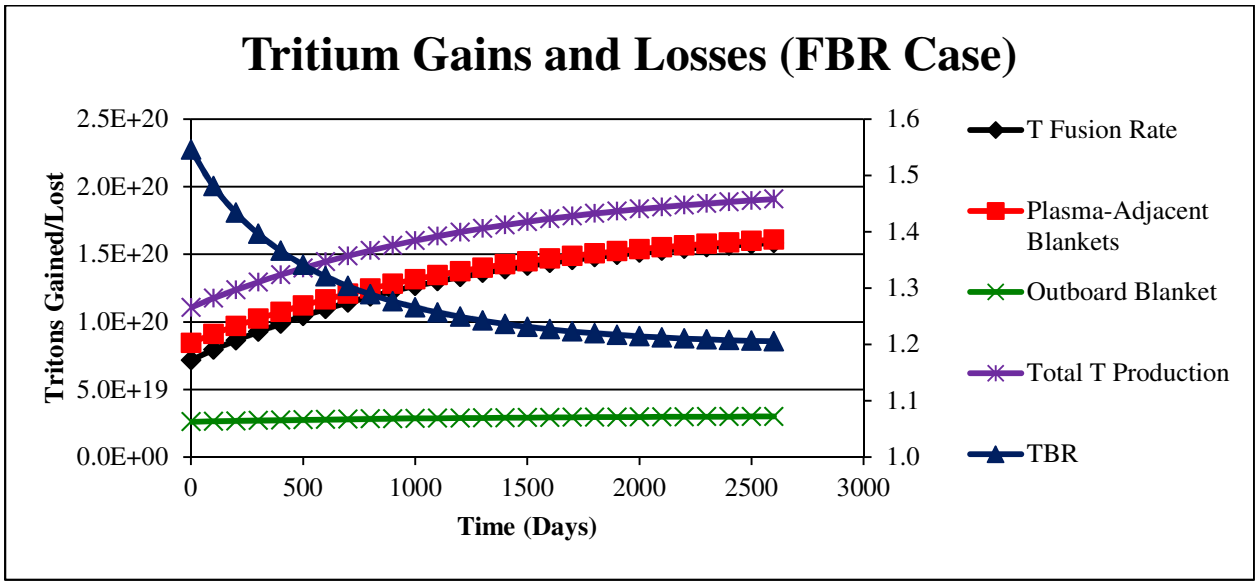

Figure 5.6: Tritium Breeding for the FBR Configuration

The net gain in the FBR case for each of the primary fissile isotopes is shown in Figure 5.7. The peak value (FBR = 1.340) occurs near day 1200 of fuel residence time, and the EoC value is 1.298. The average net fissile production rate is 253.7 kg/efpy.

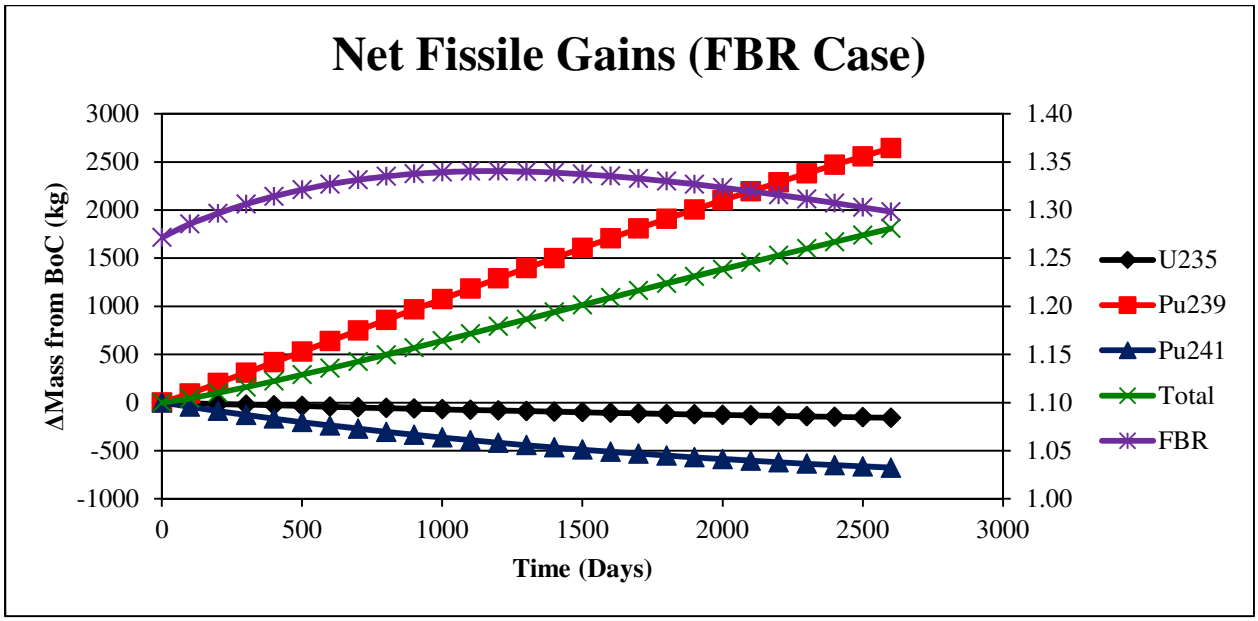

Figure 5.7: Fissile Breeding for the FBR Configuration

The driver fuel has a maximum burnup of 10.23 at%; this is higher than in the TBR case, but the peak burnup rate of the driver fuel is actually lower. The peak burnup in the radial blankets occurs in the plasma-adjacent slice, and is 2.98 at% at day 2600 of fuel residence time.

The fast fluence and DPA accumulation across the core midplane are shown in Figure 5.8 at various points throughout the fuel life; the end of cycle (EoC) occurs after 2600 days. The EoC values are given at 2600 days of fuel residence time. The maximum DPA is 124 and the maximum fast fluence is 3.12×10^{23} n/cm^2.

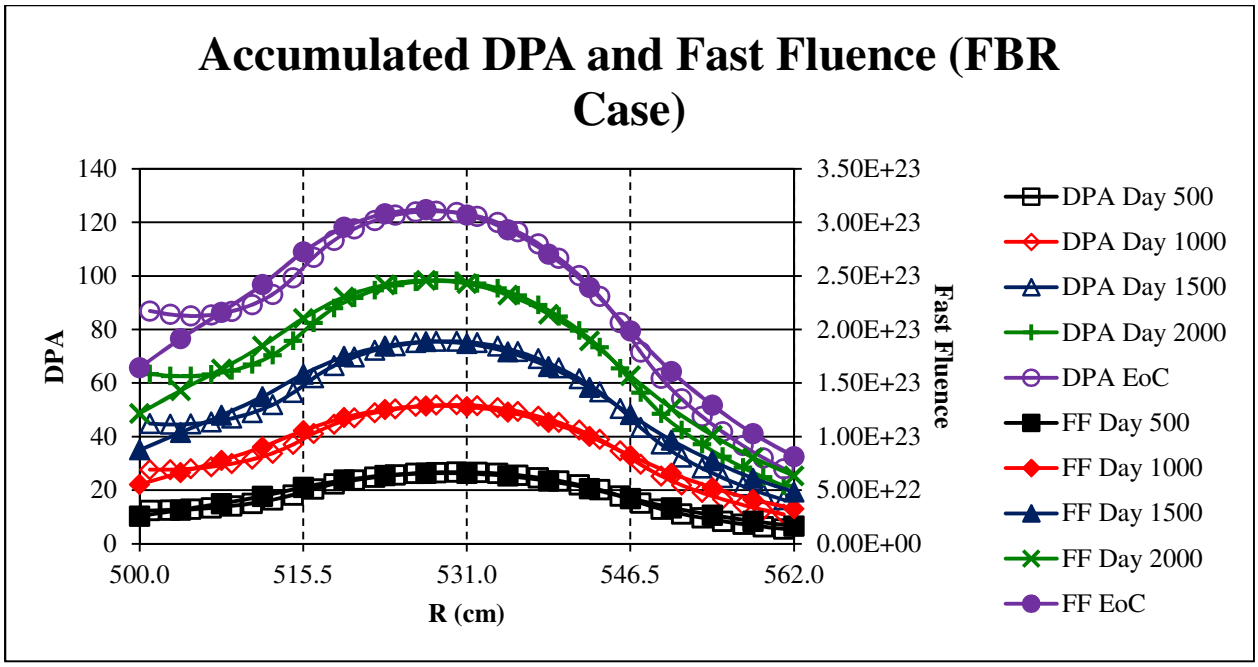

Figure 5.8: Radiation Damage for the FBR Configuration

Electrically Insulating Sheath Removed

The multiplication factors and fusion power for the unsheathed case are shown in Figure 5.9. This case began with a high k_{eff} relative to the FBR case with which it shares reflector and tritium blanket geometry. The case was run despite the initially high k_{eff} in order to compare directly with the FBR case. Contrary to both the FBR and TBR cases, no hard constraint was violated in the unsheathed case in the 2600-day fuel residence time.

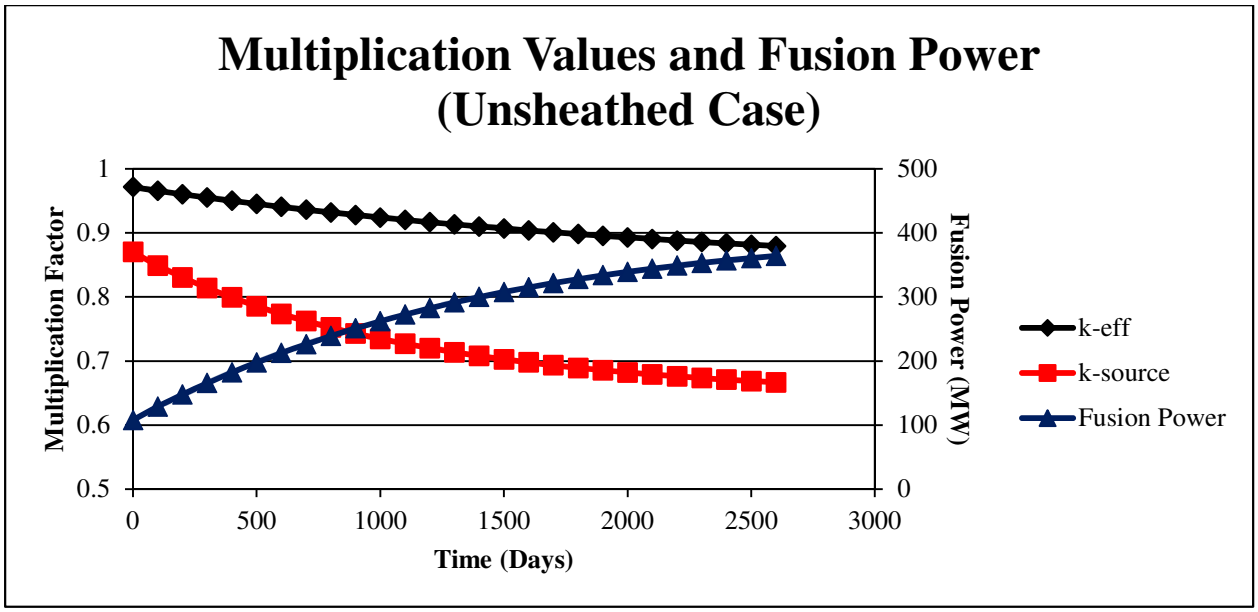

Figure 5.9: Multiplication Values and Fusion Power for Unsheathed Case

Figure 5.10 shows the tritium gains and losses for the unsheathed case. The overall shapes of the capture rates in each tritium blanket region are consistent with those from the TBR and FBR cases. However, the production rate in the plasma-adjacent blankets is noticeably higher than the consumption rate by fusion, whereas these values were nearly identical in the other cases. Though this could be explained by the higher source multiplication factor of the unsheathed case, a more likely reason is that the leakage from the core is higher. The substantially higher tritium production in the outboard tritium breeding blanket relative to the FBR case supports this interpretation of the data.

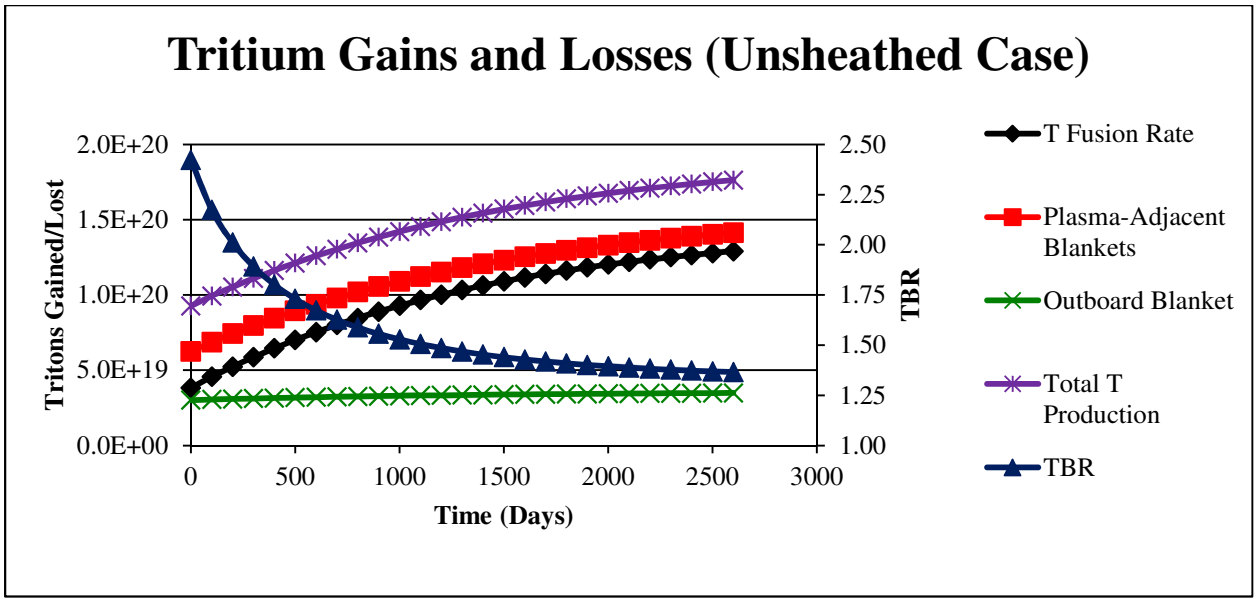

Figure 5.10: Tritium Breeding for the Unsheathed Case

Figure 5.11 shows the fissile mass gains for the unsheathed case and the fissile breeding ratio. The peak value of 1.301 occurred at day 1500 of fuel residence time, 300 days later in the cycle than in the FBR case. The fissile breeding ratio of the unsheathed case also has a greater rate of change than in the FBR case.

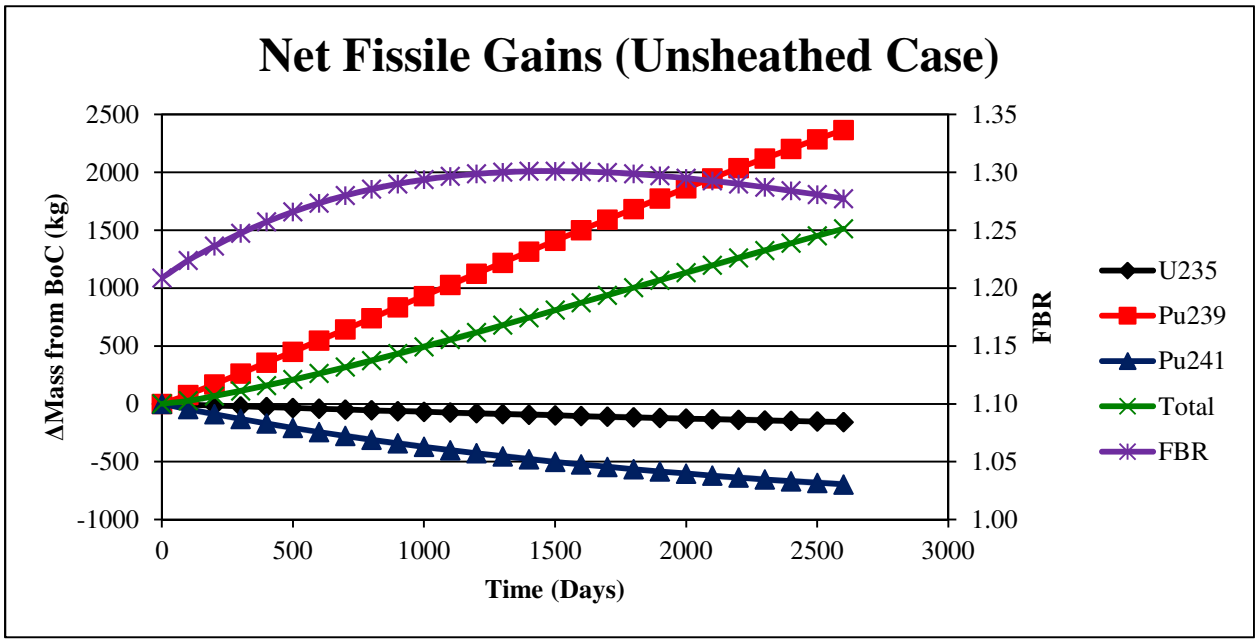

Figure 5.11: Fissile Breeding for the Unsheathed Case

The peak driver burnup in the unsheathed case was 10.48 at%, and the peak blanket burnup was 2.43 at%, indicating that more power production occurred in the driver fuel relative to the FBR case. The highest blanket burnup occurred, as in the other cases, in the plasma-adjacent edge of the ring 1 blanket assemblies. However, because of the higher driver fuel power and lower required source strength, the burnup across the blanket is relatively flat.

The accumulated radiation damage for the unsheathed case is shown in Figure 5.12. The EoC values are taken at day 2600 of fuel residence time. The peak DPA is 134, and the peak fast fluence is 3.38 n/cm^2.

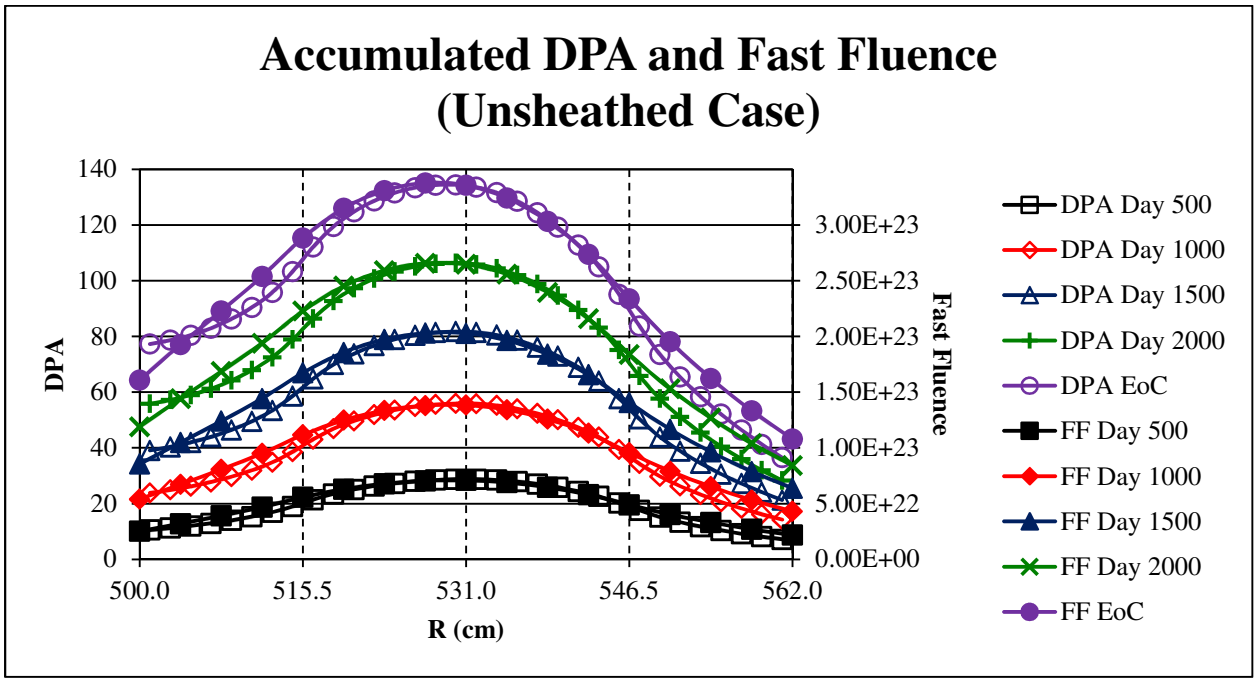

Figure 5.12: Radiation Damage for the Unsheathed Case

Depleted Uranium Loading

The case in which radial blanket assemblies were loaded into all 4 assembly rings was unable to achieve tritium self-sufficiency at the BoC. If it had been able to increase the fission annulus neutron multiplication sufficiently quickly and thereby increase production in the surrounding tritium blankets to raise the TBR above 1.15, it may have

been able to function with a large initial tritium inventory. However, this was not the case. Nonetheless, there are some results from the DU loading scenario which illustrate the effect of the fusion neutron source and of the breeding in the plasma-adjacent blankets, and the case was run to the limit of blanket burnup, which occurred after 2400 days.

Because the fusion power was kept at its maximum for the full fuel residence duration, the thermal output of the fission annulus is instead plotted along with the k_{eff} and k_{mult} in Figure 5.13 for this case. Contrary to the monotonic decrease of the multiplication constants of the other cases, the dearth of fissile mass at BoC causes very low BoC values which increase as ^{239}Pu is bred into the fission annulus. Consequently, the fission output nearly doubles over the course of the burnup cycle, although it never exceeds even ¼ of the SABR design output.

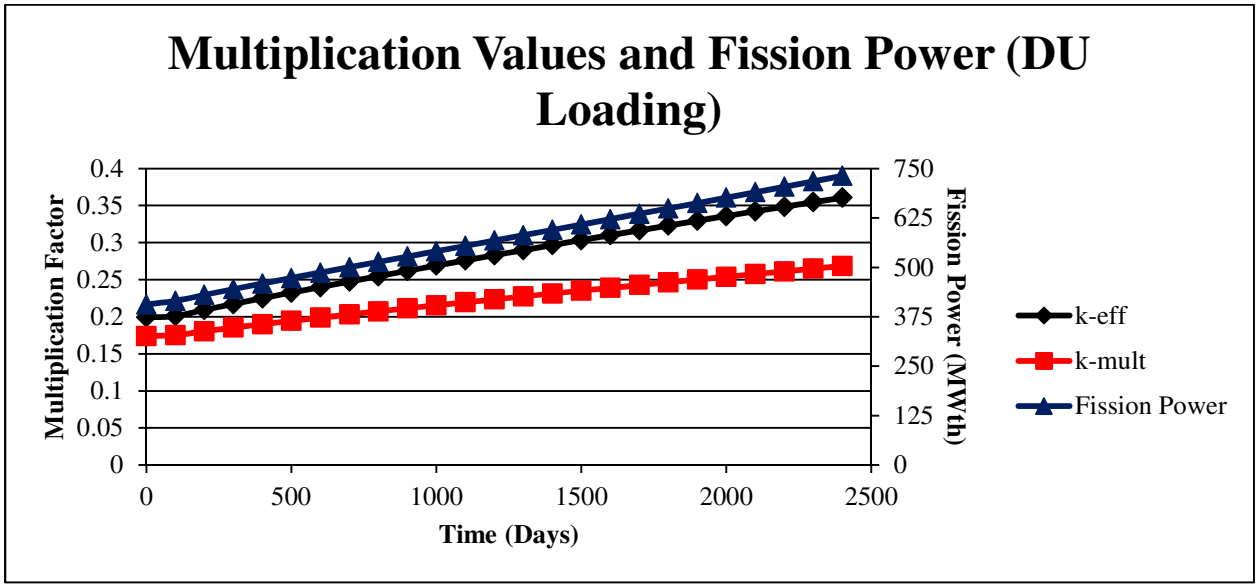

Figure 5.13: Multiplication Values and Fission Power for DU Loading

The low fission rate negatively affected tritium breeding, to the point that despite an increase of the TBR over the burnup cycle, it never achieved TBR = 1, let alone enough excess to offset losses from decay, exhaust, and separation. The tritium production in the plasma-adjacent blankets increased slowly over the burnup cycle due to

the increase in fission rate in the first fission assembly ring as ^{239}Pu was bred in. The outboard tritium breeding blanket saw relatively few of the source neutrons, and without an initial fissile loading in assembly rings 2 and 3, the fissile production rate in ring 4 was very low. As a result, the outboard blanket contributed very little to the overall tritium production at any point.

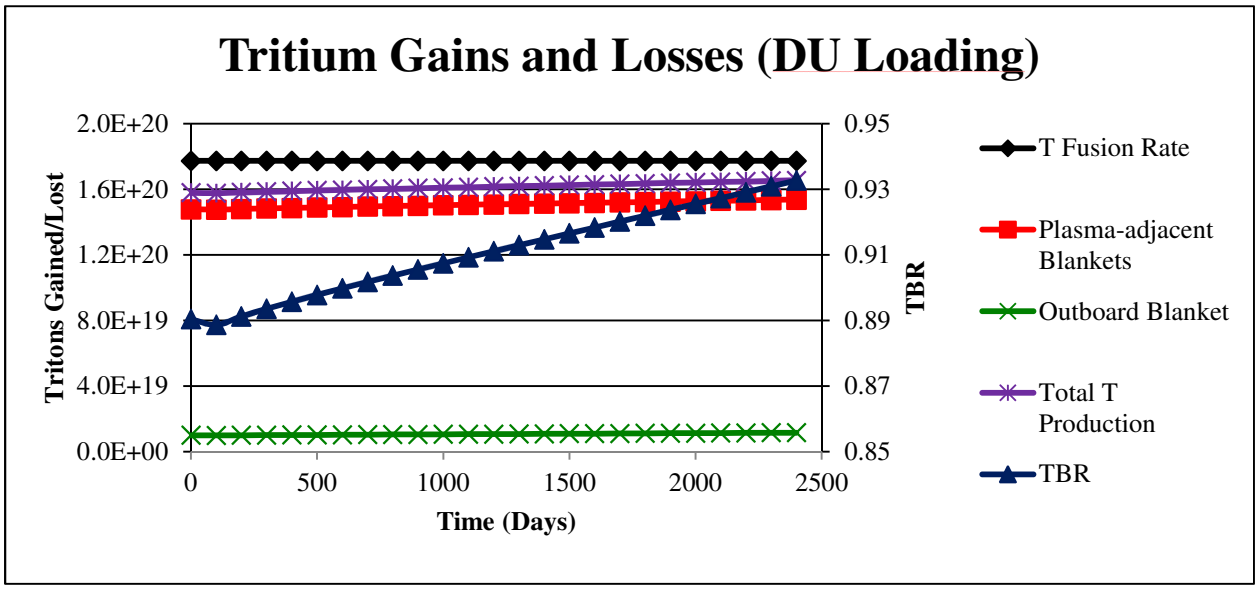

Figure 5.14: Tritium Breeding for the DU Loading

Another consequence of the low fission rate was a very different radiation damage distribution. Without a significant fission neutron flux, the shape of both the DPA and fast fluence curves resembles beam attenuation; this is to be expected, since essentially this case represents an attenuated source with a slight contribution from fission neutrons near R = 500 cm. The plasma-adjacent edge of the fission annulus incurred similar levels of damage as the same location in the other cases, but beyond the first few cm, the overall radiation damage was insignificant in comparison.

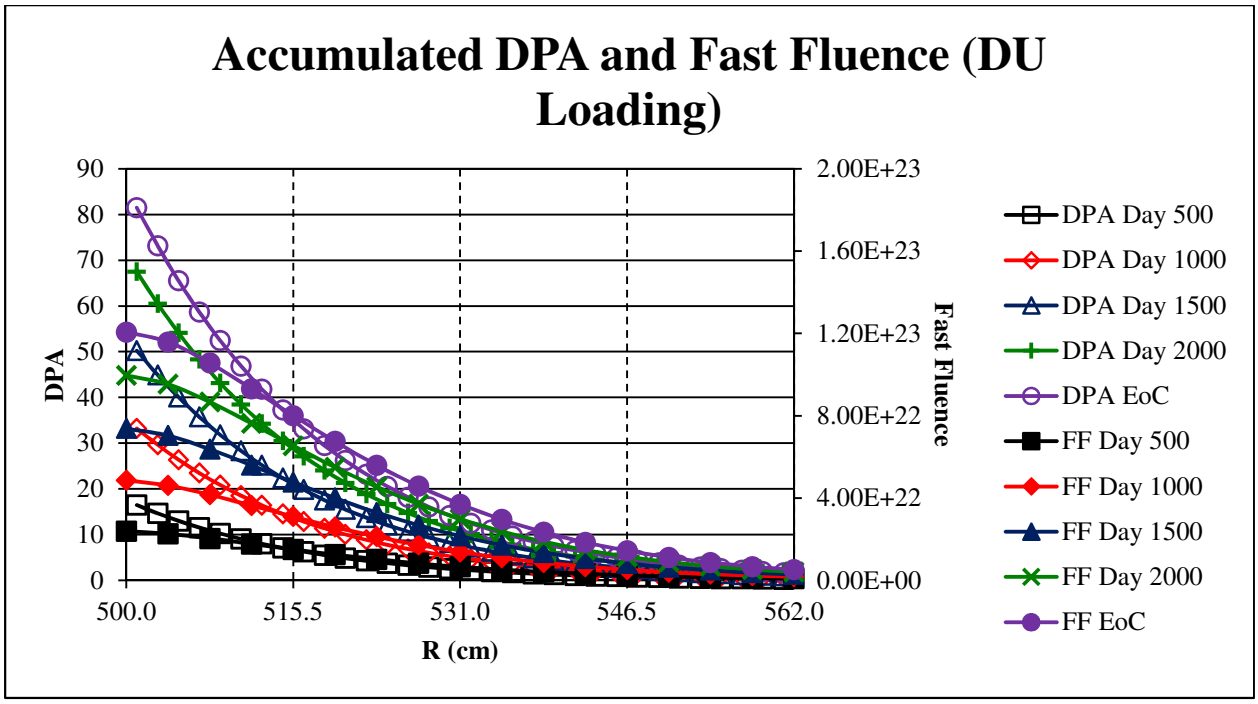

Figure 5.15: Radiation Damage for the DU Loading

The tritium breeding performance of the DU loading case demonstrates that a significant initial fissile loading is necessary to increase the TBR to acceptable levels in the SABR geometry.

CHAPTER 6

DISCUSSION

Tritium Breeding

The tritium breeding rates of the plasma-adjacent blankets closely track the neutron source strength in all of the studied cases; both increase throughout the burnup cycle. The first reason for this is that since these blankets subtend the majority of the solid angle of the neutron source region, increasing the fusion rate increases the incident flux directly. The second, indirect, reason is that leakage from the first ring of assemblies increases as the fuel is irradiated. Because the inner assembly ring of the fission annulus is composed of blanket assemblies, its fissile enrichment increases significantly throughout burnup. Furthermore, increasing the source strength causes more fusion neutrons to be incident on these fission blanket assemblies, which causes more fissions in both the fertile and bred-in fissile material there as the burnup cycle progresses.

The tritium breeding rate of the outboard blanket, on the other hand, is nearly constant throughout the burnup cycle in each of the cases. Because the breed-in of fissile material in the fission blankets in the 4^{th} assembly ring is slow compared to that in the 1^{st} ring, its fission rate does not increase nearly as much. The gradual reduction of power in the adjacent driver fuel as it burns through its initial fissile charge reduces the flux incident on the blanket, offsetting the increase in fissile enrichment in the blanket assemblies. These, coupled with the lack of an external source which increases in strength as burnup progresses, lead the capture rate in the outboard tritium breeding blanket to increase by only a few percent from the beginning to the end of cycle.

Neutron Spectra

The neutron spectra at several locations in the core for the TBR case and the FBR case are shown in Figures 6.1 and 6.2, respectively, at 1000 days into the fuel residence time. The spectra are somewhat similar throughout the fission annulus, with the hardest spectrum in the center of the fission annulus. Those in the radial fission blankets are slightly softened from the core-center spectrum; the inner radial blanket is slightly higher-energy than the outer radial blanket due to the higher mass of fissile material bred in and the scattered fusion neutrons. There is a pronounced difference between the cases in the spectra of the outboard Tritium breeding blanket. In the FBR case, in which the leakage neutrons from the fission annulus must also cross the reflector before entering the tritium breeding blanket, the higher-energy peak has mostly scattered into the lower-energy one. The un-slowed source neutrons can be seen in the highest energy group in the spectrum in the inner radial blanket only 2 cm away from the plasma (red), but this high-energy peak is noticeably absent from all of the other spectra. The similarity of the spectra throughout the fission annulus and the dearth of fusion neutrons in all but the plasma-adjacent spectrum indicate that the neutron spectrum is dominated by local material compositions rather than the external source, and that the material compositions will primarily determine radiation damage, fission-to-capture ratios, and other energy-determined phenomena in all regions except those immediately adjacent to the plasma chamber.

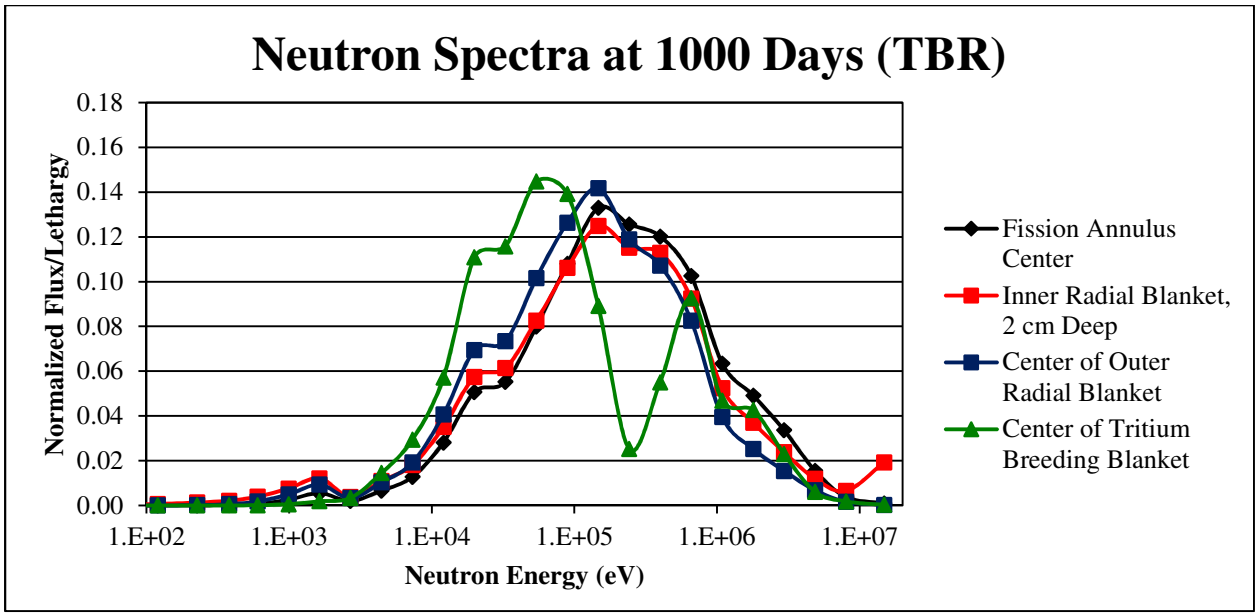

Figure 6.1: Neutron Spectra at Selected Locations (TBR Case)

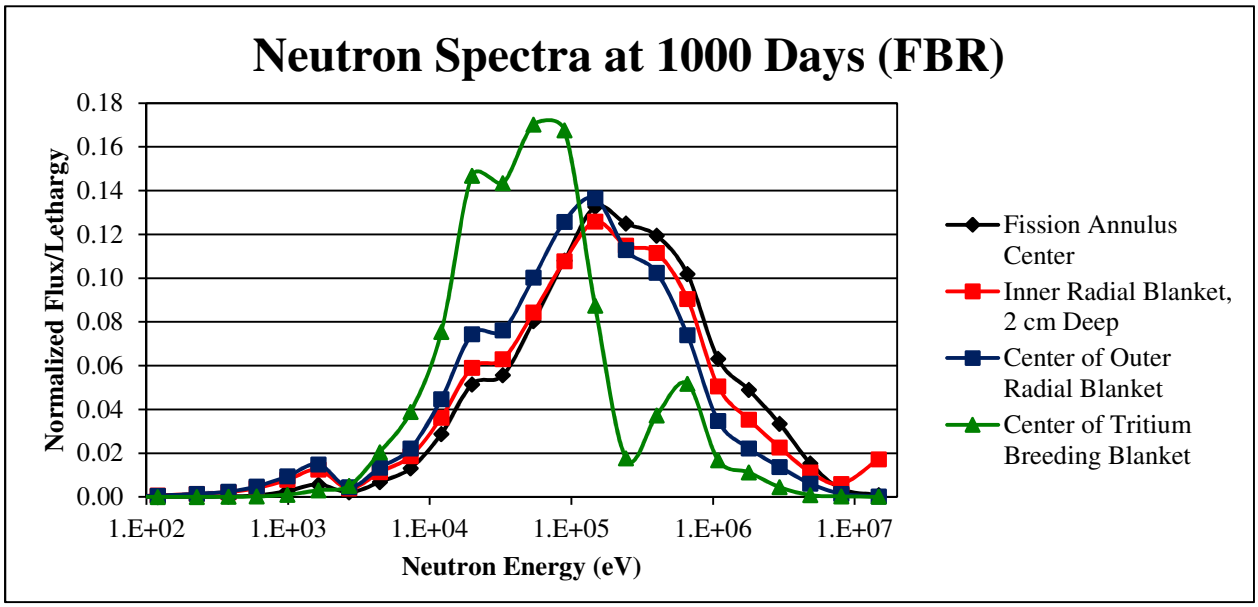

Figure 6.2: Neutron Spectra at Selected Locations (FBR Case)

The removal of the insulating $LiNbO_3$ sheath hardened the neutron spectrum somewhat, particularly in the few-hundred-keV range. The core-center spectrum comparison between the FBR case and the sheath removal case is shown below (Figure 6.3). The high-energy shoulder of the peak with the sheath removed is slightly more

populated; the reduction in the low-energy shoulder is more pronounced. Since the few-hundred-keV range is the most populous for fast reactors, shifts toward higher-energy of this peak significantly affect the reactor. The average number of neutrons released per fission increases, the fission-to-capture ratios increase, and threshold fission reactions become more prevalent. These effects, all of which increase the core's reactivity, are offset by an increase in mean free path, and therefore leakage from the reactor. Since SABrR has a particularly spoiled geometry – its fission core is very tall and thin and is annular with a large inner radius – the effects of increased leakage in traditional pancaked cylindrical geometry will be enhanced.

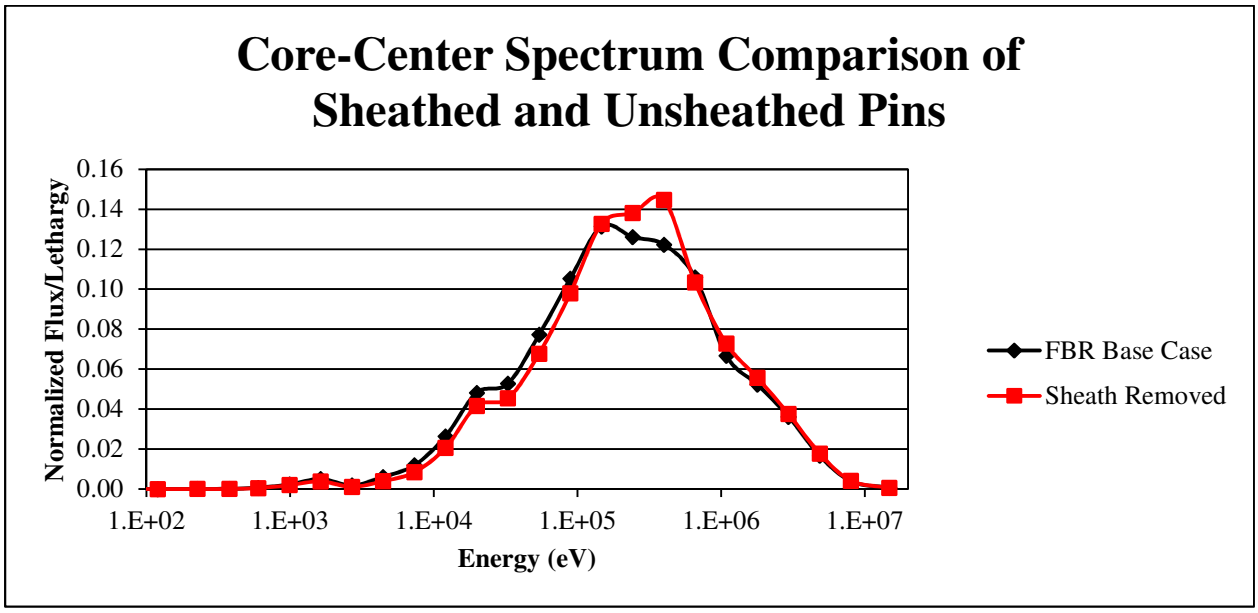

Figure 6.3: Core-Center Spectrum Comparison for Sheathed and Unsheathed Pins

Radiation Damage

The two measures of accumulated radiation damage tend to track each other very well except in the first assembly ring. In the TBR, FBR, and unsheathed cases, the fast fluence and DPA curves diverge slightly at the inboard edge of the driver fuel in ring 2; this divergence becomes more pronounced, and quite significant, toward the plasma-adjacent edge of ring 1. The fusion neutrons – at 14.1 MeV – are far more damaging to

the cladding than the average fission neutron, so the DPA curve turns upward as it approaches the plasma. The fusion neutron component of the radiation damage falls off as the distance from the plasma increases and the source neutrons are down-scattered or absorbed. This can be most easily identified in the radiation damage figure for the DU loading (Figure 5.15), as the fusion neutrons cause the majority of the radiation damage in this case. On the other hand, since fast fluence tallies all neutrons above 0.1 MeV equally regardless of their energy, the fusion-born neutrons do not count more than those born by fission. Since in the fission annulus the total number of fission neutrons far exceeds the number of fusion neutrons, the fast fluence curve falls off similar to a chopped cosine as it approaches the plasma-side boundary of the annulus. For this reason, DPA is superior to fast fluence as a measure of radiation damage to the cladding for the study of SABrR.

The peak values of both fast fluence and accumulated DPA in all cases but the DU loading occur in the driver region. This is because, as mentioned, the fission-born neutrons far outnumber the fusion neutrons, and thus out-compete their damage contribution despite their higher damage caused per collision. The exact radial location of maximum radiation damage shifts slightly inward as burnup progresses; both the increasing strength of the neutron source on the inboard side of the annulus and the higher fissile breeding rate and power production of the ring 1 blanket assemblies contribute to this shift. Since both of these effects are most pronounced in the TBR case and less so in the FBR and unsheathed cases, the rate of the shift is correspondingly higher.

The radiation damage in the ring 4 blanket assemblies is significant (60-90 DPA, depending on the case) on the edge directly adjacent to the driver fuel, but falls off precipitously across the assembly ring. This is expected given the arrangement of the multiplying media and the lack of an external source on that edge of the annulus. A divergence between the accumulated fast fluence and DPA curves can be seen on this

edge of the annulus as well, although it is not as extreme as that in ring 1. The primary reason for the divergence is that the reflected and somewhat moderated neutrons returning from the adjacent outboard media (whether reflector or tritium breeding blanket) reduce the average neutron energy relative to the average in the driver fuel. However, because a significant fraction of the reflected neutrons have energies in excess of 0.1 MeV, they are still tallied in the fast fluence despite being less damaging on average.

Power Distribution

The distribution of power produced in the driver and in the blankets changes significantly as burnup progresses. Initially, the driver fuel produces nearly all of the fission power, but as fissile isotopes are depleted from the driver fuel and bred in the breeder blankets, the blankets produce an increasing fraction of the power. This increase in blanket power is more pronounced in the inner radial blanket assemblies than the outer ones, as they are exposed directly to the fusion neutron source and thus have a higher rate of breeding and a high incident neutron flux from the plasma. The radial power profiles across the core midplane for the TBR and FBR cases are shown in Figures 6.4 and 6.5, respectively for BoC, 1000 and 2000 days of fuel residence time, and EoC. The data for power in each case is normalized to the maximum power across the entire burnup cycle for that case. The larger difference in the FBR case of the curves for 2000 days and EoC is due to the longer cycle duration rather than any geometry-related phenomena.

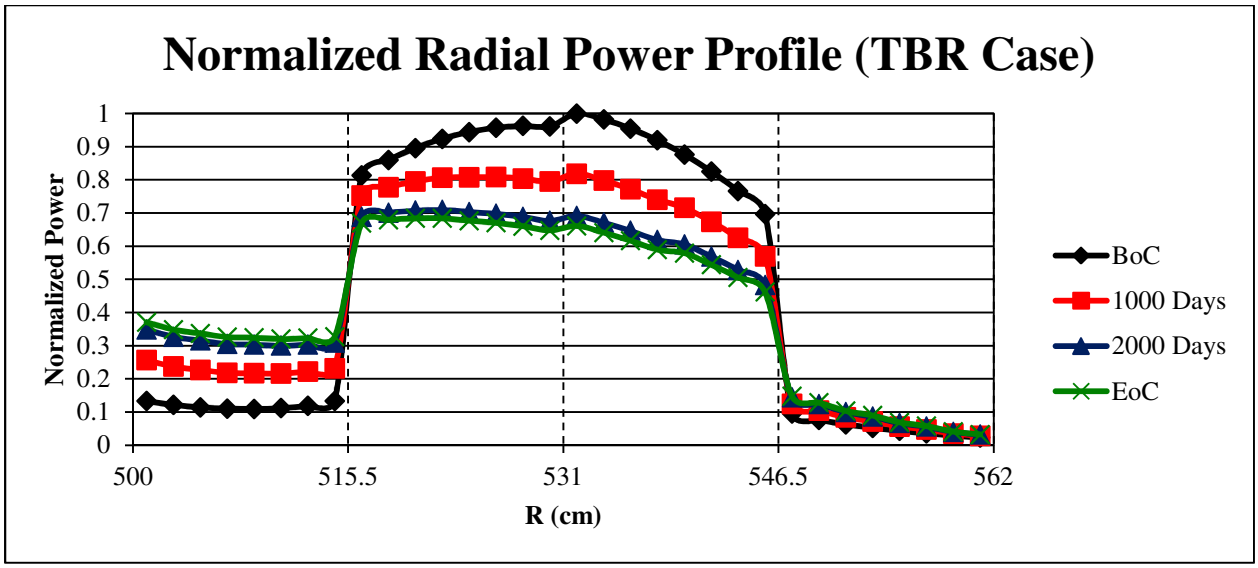

Figure 6.4: Radial Power Profiles for the TBR Case

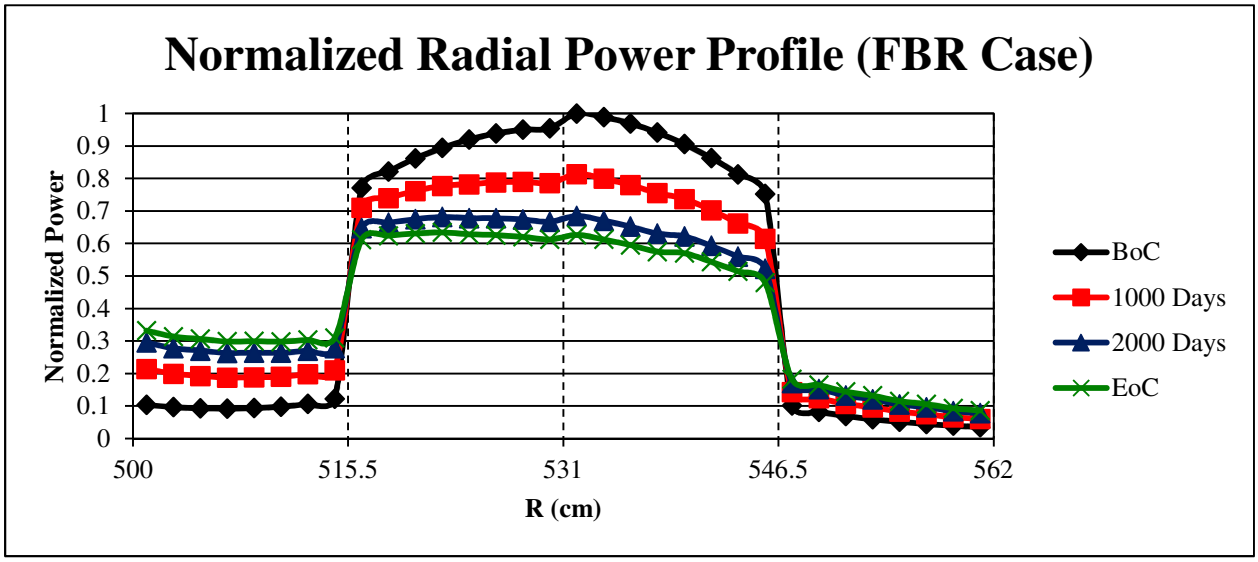

Figure 6.5: Radial Power Profiles for the FBR Case

The shape and evolution of the power generated in the driver fuel is similar across both cases, with power initially peaked in the center of the annulus and transitioning toward the plasma as burnup progresses. The power generated in the ring 1 fission blankets is initially very similar between the cases, but increases faster in the TBR case than the FBR case to the extent that the 2000-day curve in the first assembly ring for the

TBR case roughly aligns with the EoC curve for the FBR case, despite occurring 600 days earlier in the cycle. The higher required fusion source strength in the TBR case is responsible, causing both faster breed-in of fissile material in the first assembly ring and greater energy deposit from scattering of the source neutrons; the greater upward curvature of the TBR case at R = 500 cm supports this interpretation. Conversely, the power in the ring 4 blankets increases faster in the FBR case. The reasons are threefold: first, the albedo of the adjacent outboard material is higher; second, there is no competing capture reaction in the adjacent media that rivals that of ^{6}Li; and third, the adjacent driver fuel (in ring 3) sustains a higher power level throughout the burnup cycle. These three all cause the FBR case to have a higher flux and more breed-in of fissile material in the outboard blanket ring.

Fission-to-Capture Ratios

The fission-to-capture ratios of the three cases which had initial fissile charge show behavior that differs by isotope and annulus region in a way that illustrate the high leakage of the annular core and the effect of the fusion neutron source. The ^{239}Pu ratios of the fission annulus for the TBR, FBR, and unsheathed cases are shown in Figure 6.6.

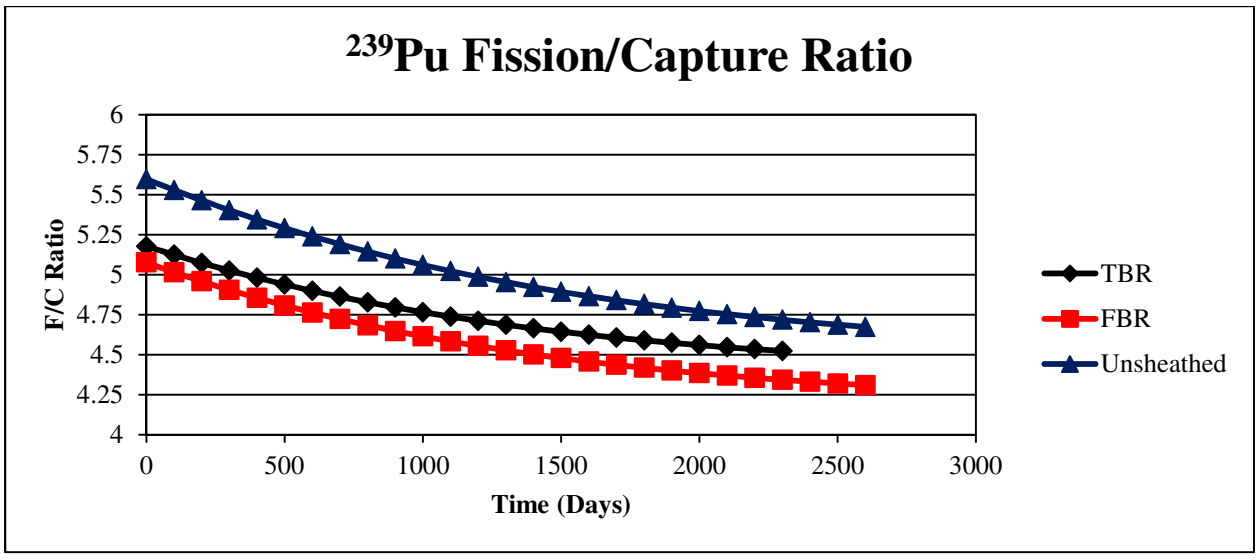

Figure 6.6: ^{239}Pu Fission-to-Capture Ratios for the Fission Annulus

All three cases show a similar decrease of the fission-to-capture ratio as burnup increases. Initially, all of the ^{239}Pu lies in the driver region. As the driver Pu charge is depleted and more is bred into the blankets, the average number of scattering events a neutron undergoes before being absorbed by a ^{239}Pu nucleus increases. For the blankets this is particularly true due to the very low atomic concentration of ^{239}Pu among the ^{238}U; as more Pu is bred into the blankets and the flux in the annulus becomes spatially flatter, the blankets figure more heavily into the averaging for the ratio.

At any given point in time, the ratio of the unsheathed case is higher than that of the TBR case, which is in turn higher than the FBR case. The harder neutron spectrum of the unsheathed case due to its lack of moderation by $LiNbO_3$ is responsible for its superior performance in this regard. The TBR case ratio exceeds the FBR case ratio primarily because of the higher fusion source strength and because the ^{6}Li adjacent to the ring 4 blankets competes with the heavy metal isotopes there for capture of lower-energy neutrons. These two effects are more noticeable in their respective adjacent blanket rings, but serve to slightly harden the spectrum of the TBR case relative to the FBR case throughout the annulus.

The fission-to-capture ratios of ^{240}Pu and ^{241}Pu show similar traits to the ^{239}Pu ratios; since they initially exist only in the driver fuel and are bred into the blankets as their driver charge depletes, the same physical phenomena and averaging processes apply to them. The advantage of the unsheathed case is slightly more pronounced in these due to the much lower production rate of these isotopes in the blanket fuel, but the TBR and FBR cases show a similar-percent difference. The effect of the core-center spectral differences in the 3 cases are illustrated by the ^{239}Pu ratios averaged only the driver fuel (Figure 6.7); leakage effects from the fission annulus are suppressed by this choice of averaging. With the blanket contribution removed, the TBR and FBR cases track each other more closely, because while their peripheral geometry differs, their geometry and initial material compositions are identical in the fission annulus.

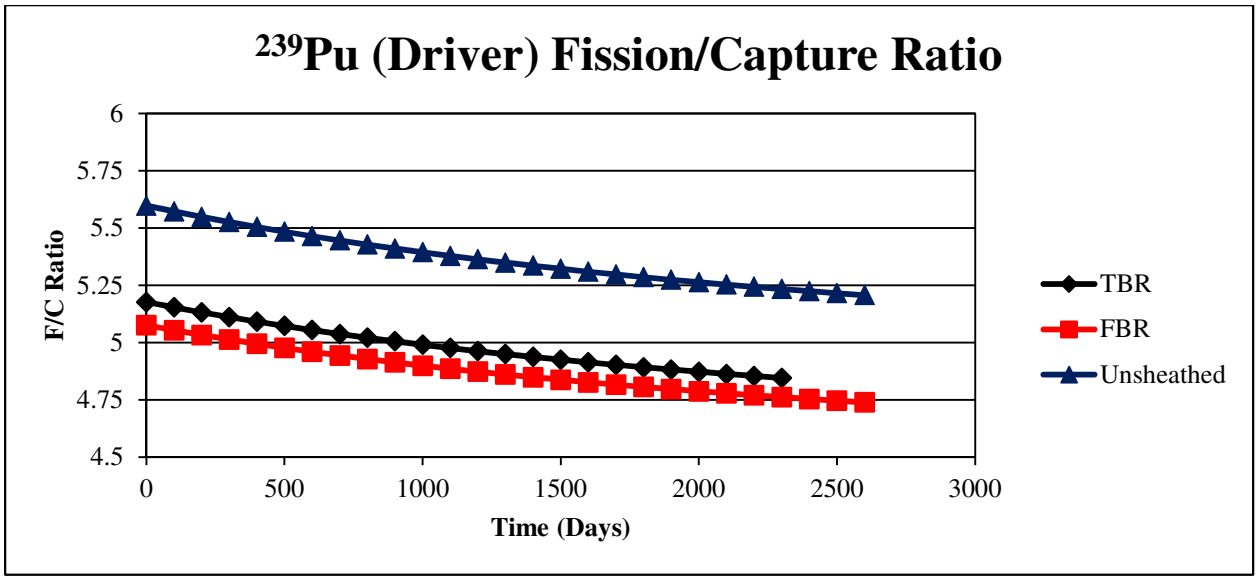

Figure 6.7: ^{239}Pu Fission-to-Capture Ratios for the Driver Fuel Only

In contrast, the ^{238}U fission-to-capture ratios (Figure 6.8) demonstrate the effect of implicitly weighting by isotopic density and flux and the importance of the fusion neutron source to the neutronics of the adjacent blanket material. Because the smeared density of the fuel pins is 85% in the blanket assemblies and only 75% in the driver assemblies, the blanket assemblies have a higher isotopic fraction of ^{238}U, and the ring 1 blanket receives flux contributions from both the driver fuel in ring 2 and the neutron source, the fission-to-capture ratios for the annulus are very dependent on the ratios in the first assembly ring. The plasma contributes to the neutron spectrum in this ring enough that the fission-to-capture ratio of the TBR case exceeds that of the unsheathed case; the FBR case is still the lowest throughout the burnup cycle. The increase with burnup in the ratios of all 3 cases is due to the monotonically increasing source strength, and to a lesser extent, the increasing fission rate in the ring 1 blanket as more fissile material is bred in.

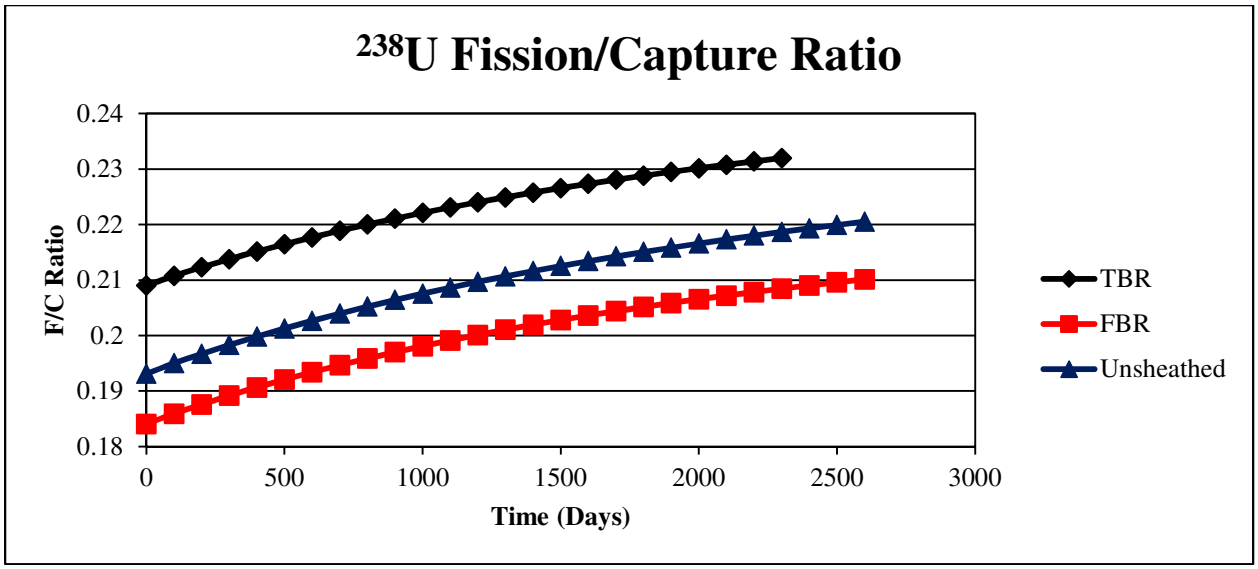

Figure 6.8: ^{238}U Fission-to-Capture Ratios for the Fission Annulus

Breeding Comparison to Critical Fast Reactor

A comparison of the breeding performance of SABrR with the high-breeding metal-fueled S-PRISM core design[18] from which the SABrR fuel pins were adapted is shown in Table 6.1. This critical system was chosen for the comparison because of the pin similarity and because of the maturity of the S-PRISM design. Because breeding performance is sensitive to the neutron spectrum and the spectrum of a fast reactor is very sensitive to the volume fractions of the fuel, structure, and coolant in its core, a side-by-side comparison of the SABrR and S-PRISM pin and assembly dimensions and smeared volume fractions is included in Table 6.2.

Table 6.1: Breeding Performance Comparison of SABrR to S-PRISM

Quantity	SABrR	S-PRISM
Core Thermal Power (MW)	3000	1000
BoC TRU Loading (kg)	14317.0	3159.9
BoC Fissile Pu Loading (kg)	9738.2	2458.8
BoC U Loading (kg)	164763.1	33052.7
Specific Power (W/gTRU)	209.54	316.47
TRU Enrichment (wt%, TRU/(U+TRU))	Driver Zone 1 – 22.36 Driver Zone 2 – 23.75	21.29

	TBR Case	FBR Case	Unsheathed	-
Fuel Residence Time (days)	2300	2600	2600	Driver – 2070 Blanket – 2760
Cycle-Average Breeding Ratio	1.28	1.32	1.28	1.22
Fissile Gain (kg/year)	208.39	253.73	212.37	69.91
Normalized Fissile Gain (kg/(MW_{th}*year)	0.0695	0.0846	0.0708	0.0699

Table 6.2: Pin and Assembly Dimensions and Volume Fractions of SABrR and S-PRISM

Quantity	**S-PRISM Metal Core**		**SABrR**	
Assembly Type	**Fuel (cm)**	**Blanket (cm)**	**Fuel (cm)**	**Blanket (cm)**
Assembly Pitch	16.142	16.142	16.3	16.3
Duct Gap	0.432	0.432	0.6	0.6
Duct Wall Thickness	0.394	0.394	0.1	0.1
Pin Count	271	127	271	271
Pin OD	0.744	1.201	0.744	0.744
Cladding Thickness	0.0559	0.0559	0.056	0.056
Fuel OD	0.5477	1.046	0.5477	0.5827
Pin Spacer Type	Wire Wrap		Wire Wrap	
Spacer Wire Diameter	0.1422	0.940	0.1230	0.1230
Fuel Fab Density (%TD)	100	100	100	100
Fuel Smear Density (%TD)	75	85	75	85
Volume Fractions (%)				
Fuel	28.30	44.61	27.71	31.41
Bond	9.43	7.87	9.24	5.54
Coolant	36.57	26.54	36.46	36.46
Structure (Clad, Duct, Spacer)	25.70	20.97	18.00	18.00
$LiNbO_3$ Sheath	--	--	8.59	8.59

The lower specific power and higher TRU loading of SABrR are a direct consequence of the annular geometry of its fission core; such geometry has a much higher leakage than the traditional pancaked cylinder, so the driver fuel k_∞ must be correspondingly higher even for a lower k_{eff}. The higher fissile loading of SABrR means that despite its higher fissile breeding ratio, it has a longer doubling time. However, the

fissile gain normalized to fission core thermal power is roughly equal for the SABrR TBR case and S-PRISM, while the SABrR FBR case exceeds S-PRISM in this regard.

SABrR has a higher fuel residence duration than S-PRISM's driver fuel, but a slightly lower blanket residence time. This S-PRISM core design is radially heterogeneous and utilizes blanket shuffling to flatten the radial power profile. SABrR, however, does not shuffle assemblies at any point during the burnup cycle – the presence of the neutron source at the edge of the fission annulus and the ability to adjust its strength largely negate the need to do so for power flattening purposes. Therefore, SABrR would be shut down far less frequently for shuffling/refueling purposes – an advantage it holds over nearly all critical systems.

Because cycle length for both the FBR and TBR cases for SABrR were limited by blanket burnup in ring 1 with reasonable margin to peak radiation damage and driver burnup limits, the radial blankets in rings 1 and 4 might be switched mid-residence time in order to increase total residence time, although at the cost of increased downtime. Finding a suitable electrically insulating material which has less moderating power than the $LiNbO_3$ would also extend the cycle duration of SABrR since the blanket burnup limit was not reached in that scenario. A less-moderating insulator would allow for either decreased fissile enrichment of the driver fuel or for radially heterogeneous core layouts which do not increase driver enrichment to high levels.

CHAPTER 7

CONCLUSION

The SABR fission-fusion hybrid fast burner reactor concept, based on IFR/S-PRISM fast reactor physics and technology and on ITER fusion physics and technology, was investigated for a fast breeder reactor application. Representative configurations of the annular fission core and its surrounding structures were considered for the ability of SABrR to breed fissile material from depleted Uranium while simultaneously breeding Tritium, subject to realistic constraints on i) the radiation damage to the cladding (200 DPA or $4x10^{23}$ n/cm^2 fast fluence), ii) driver fuel burnup (13.33 at%), iii) blanket fuel burnup (3 at%), and iv) tritium self-sufficiency (TBR > 1.15). The representative designs considered were found to be capable of producing fissile breeding ratios of about 1.3 and maintaining Tritium breeding ratios greater than 1.2. This neutron economy is sufficient to produce about 250 kg/yr of fissile material in a 3000 MW_{th} plant while also producing enough tritium for self-sufficiency of the fusion neutron source fuel.

Although the TBR configuration bumped up against the limit of the fusion neutron source to drive the fission annulus at 3000 MW_{th}, the key limiting factor for cycle length in both the TBR and FBR configurations was burnup of the plasma-adjacent blanket material. There are several measures which could be taken to address this and extend the blanket lifetime of SABrR, each with different consequences for breeding performance and the economy of the overall fuel cycle. The two options which would change the least about the design of SABrR are likely to be blanket shuffling and replacement of the $LiNbO_3$ insulating sheath with a less-moderating insulator; these would both bring the blanket burnup timescale close to that of the cladding radiation damage limit. For any cycle which utilized assembly shuffling, an important consideration is to align the shuffling and refueling times with the replacement interval

for the first wall of the plasma chamber. Current estimates for the SABR first wall lifetime are ~6 full-power years, but advances in materials in the coming decades and the experience gained from ITER will likely change this. The variability makes establishing a fixed cycle length for the optimization of a SABrR fuel cycle difficult and a somewhat futile endeavor this far in advance of the earliest projected readiness of the reactor.

Despite the lack of fuel-cycle optimization, SABrR compared favorably with a similarly-fueled S-PRISM core design with a high-breeding mission in terms of cycle-averaged breeding ratio, fissile production per unit energy produced, and frequency of refueling downtime. However, these advantages are likely offset by SABrR's lower specific power, which burdens it with a much higher fissile loading and a longer doubling time despite its higher breeding ratio. SABrR may also have fusion-system reasons for reactor downtime which would not affect a critical system, although with the accumulation of operation and design experience in ITER, this may be relatively small. The margins to tritium self-sufficiency, peak radiation damage, and driver fuel burnup indicate that there is room for optimization of the SABrR fuel cycle which may further extend its fuel residence time without shuffling or refueling. However, as noted above, such optimization – while useful for a near-future implementation of reactors – would be premature at this point.

In order for SABrR to compete economically with a critical FBR system, it will likely have to either demonstrate a more significant breeding performance advantage than has been determined thus far or a significant safety advantage to justify the increased complexity of coupling a fast reactor to a fusion neutron source. Such a possible safety advantage may come from an improved sodium-void reactivity coefficient which has been seen in other annular fast reactor cores; however the safety analysis of the SABrR core has yet to be performed. It is likely that the advantages may not be enough to justify the construction of a SABR-like FFH for the sole purpose of fissile breeding. A more plausible scenario is the construction of a TRU-burner SABR whose breeding/burning

mission may change as cheaply accessible fissile uranium becomes scarce and breeding becomes economically favorable. This study has established that the SABR geometry is capable of fulfilling such a purpose.

This research is being performed using funding received from the DOE Office of Nuclear Energy's Nuclear Energy University Programs.

APPENDIX A

GENERATION OF MACROSCOPIC DPA CROSS-SECTIONS

Damage to fuel pin cladding during normal reactor operation occurs primarily through atomic displacements from the crystal lattice. The accumulation of neutron-induced displacement damage is therefore an important metric in determining the lifetime of fuel elements in a fast reactor. The rate of damage accumulation is represented in a DPA cross section which is a function of the isotopic composition in the cladding and the neutron energy spectrum. ERANOS cannot produce DPA cross sections; they must either be supplied by the user within the ECCO module or modified afterward via a correction command [26]. However, ECCO can be used to obtain self-shielded microscopic cross sections which are used to produce the macroscopic DPA cross-sections.

ECCO was used to calculate energy self-shielded microscopic cross sections for each group for each of the primary isotopes in the cladding. Displacement damage data was only available for the main isotopes of Fe and Cr, but since these compose about 99% of the cladding, the calculated values are taken to be representative of the whole. For each isotope, a damage value was given in the ERANOS libraries for a capture, elastic scatter, and inelastic scatter of a neutron in each broad energy group. Within each group *g*, the microscopic DPA cross-section for each cladding isotope *i* is calculated as:

$$DPA_i^g = dpa_{cap}^g \sigma_{cap}^g + dpa_{el}^g \sigma_{el}^g + dpa_{inel}^g \sigma_{inel}^g \tag{A.1}$$

The macroscopic DPA cross-sections for each are then produced similarly to those for the other reactions:

$$DPA^{g} = \frac{\sum_{i} DPA_{i}^{g} N_{i}}{\sum_{i} N_{i}} \tag{A.2}$$

The resulting macroscopic DPA cross-sections, shown for each energy group in Table A.1., are multiplied by the neutron flux at position **r** and summed over all 33 energy groups to yield the damage accumulation rate in DPA/sec in the cladding at that position:

$$DamageRate(\mathbf{r},t) = \sum_{g=1}^{33} DPA^{g}(\mathbf{r})\phi^{g}(\mathbf{r},t) \tag{A.3}$$

This damage rate is then integrated over the core residence time to obtain the accumulated damage to the cladding (in DPA) at time τ.

$$Damage(\mathbf{r}) = \int_{0}^{\tau} DamageRate(\mathbf{r},t)\,dt \tag{A.4}$$

The calculated macroscopic DPA cross-sections which were used in SABrR show good agreement with those obtained at ANL [27] (Figure A.1).

Table A.1: Macroscopic DPA Cross-Sections

Energy Group	Midpoint (eV)	DPA (disp*barn/atom)
1	1.482000E+07	2318.704151
2	8.032650E+06	2111.039543
3	4.872050E+06	1607.070673
4	2.955050E+06	1222.224585
5	1.792350E+06	854.236781
6	1.087125E+06	562.6361549
7	6.593600E+05	426.8034127
8	3.999200E+05	318.8123944
9	2.425650E+05	197.8196144
10	1.471250E+05	135.1159088
11	8.923450E+04	106.450435
12	5.412350E+04	63.74749625
13	3.282800E+04	84.95195705
14	1.991100E+04	11.06426755
15	1.207640E+04	16.73644147
16	7.324800E+03	30.9123433
17	4.442700E+03	13.52346172
18	2.694650E+03	5.806152844
19	1.634400E+03	3.64843162
20	9.913100E+02	2.976928121
21	6.012600E+02	0.994905059
22	3.791600E+02	0.147365533
23	2.264750E+02	0.127014834
24	1.201455E+02	0.182737133
25	7.978250E+01	0.230159186
26	5.403650E+01	0.279951901
27	3.138600E+01	0.370278816
28	1.815650E+01	0.494077867
29	1.101265E+01	0.644004249
30	6.157650E+00	0.881248322
31	2.270000E+00	2.771849623
32	3.200000E-01	4.94461471
33	5.000000E-02	15.63160507

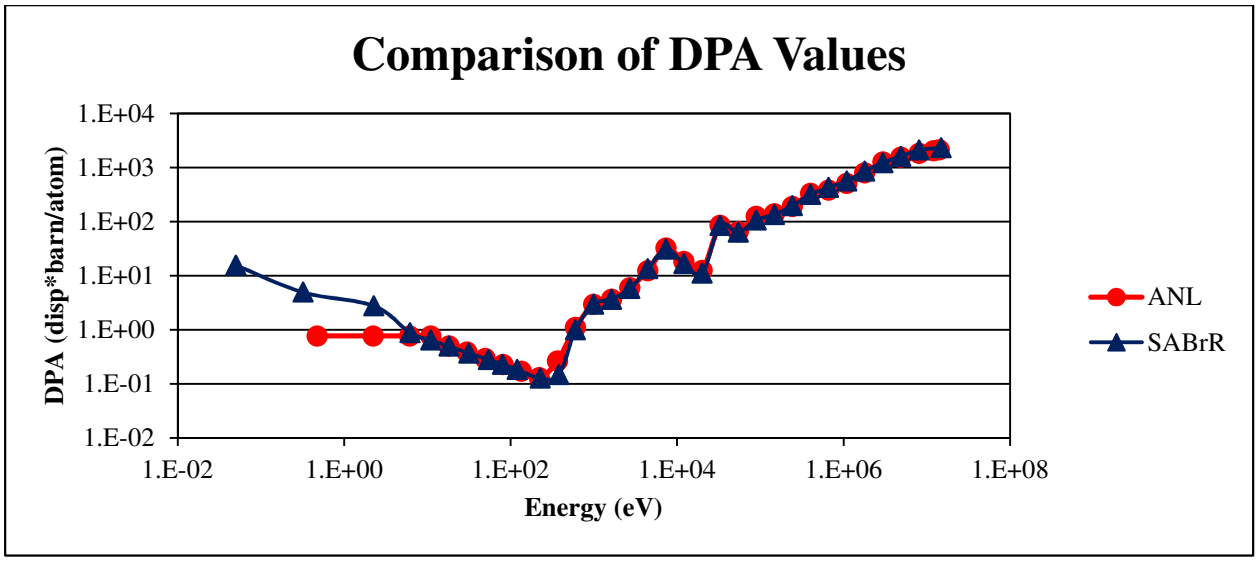

Figure A.1: Comparison of Cladding DPA Cross-Sections between ANL and SABrR

REFERENCES

1. R. D. VAUGHAN, "Uranium Conservation and the Role of the Gas Cooled Fast Breeder Reactor," *J. Br. Nucl. Energy Soc.,* **14**, 105 (1975).

2. G. A. VENDRYES, "Superphénix: A Full-Scale Breeder Reactor," *Sci. Am.*, **236**, 26 (1977).

3. Y. I. CHANG et al, "Advanced Burner Test Reactor Preconceptual Design Report," No. ANL-ABR-1, Argonne National Laboratory, (2008).

4. E. A. HOFFMAN, W. S. YANG, and R. N. HILL, "Preliminary Core Design Studies for the Advanced Burner Reactor Over a Wide Range of Conversion Ratios," No. ANL-AFCI-177, Argonne National Laboratory, (2008).

5. A. ROMANO, P. HEJZLAR, and N. E. TODREAS, "Fertile-Free Fast Lead-Cooled Incinerators for Efficient Actinide Burning." *Nuclear* Technology, **147**, 368 (2004).

6. C. E. TILL, Y. I. CHANG, and W. H. HANNUM, "The Integral Fast Reactor – An Overview," *Progress in Nuclear Energy*, **31**, 3 (1997).

7. C. E. TILL and Y. I. CHANG, "Plentiful Energy: The Story of the Integral Fast Reactor," CreateSpace, (2011).

8. H. CHOI and A. BAXTER, "A Comparative Study on Recycling Spent Fuels in Gas-Cooled Fast Reactors," *Annals of Nuclear Energy*, **37**, 723 (2010).

9. S. PIET, T. BJORNARD, B. DIXON, D. GOMBERT, C. LAWS, and G. MATTHERN, "Which Elements Should Be Recycled for a Comprehensive Fuel Cycle?," *Proceedings of Global 2007 Advanced Nuclear Fuel Cycle and Systems*, Idaho National Laboratory, Boise, ID, September 2007 (also cataloged as INL/CON-07-12197).

10. R. N. HILL, T. A. TAIWO, J. A. STILLMAN, D. J. GRAZIANO, D. R. BENNET, H. TRELLUE, M. TODOSOW, W. G. HALSEY, and A. BAXTER, "Multiple Tier Fuel Cycle Studies for Waste Transmutation," *Proc. 10th Int. Conf. Nuclear Engineering (ICONE 10)*, Arlington, Virginia, April 14–18, 2002.

11. J. P. ACKERMAN, T. R. JOHNSON, L. S. H. CHOW, E. L. CARLS, W. H. HANNUM, and J. J. LAIDLER, "Treatment of Wastes in the IFR Fuel Cycle," *Progress in Nuclear Energy*, **31**, 141 (1997)

12. W. M. STACEY et al., "A TRU-Zr Metal-Fuel Sodium-Cooled Fast Subcritical Advanced Burner Reactor," *Nucl. Technol.*, **162**, 53 (2008).

13. W. M. STACEY, "Principles and Rationale of the Fusion-Fission Hybrid Burner Reactor," Proc. FUNFI-2011 Workshop on Fusion for Neutrons and Sub-critical Nuclear Fission, Varenna, *AIP Conf. Proc*. **1442**, 31 (2012).

14. C. M. SOMMER, W. M. STACEY, and B. PETROVIC, "Fuel Cycle Analysis of the SABR Subcritical Transmutation Reactor Concept," *Nucl. Technol.*, **172**, 48 (2010).

15. W. M. STACEY, C. M. SOMMER, B. PETROVIC and C. L. STEWART, "Fuel Cycle Analysis of the SABR Transmutation Reactor for Transuranic and Minor Actinide Burning Fuels," Nucl. Technol., to be published (2012).

16. R. W. MOIR, "The Fusion Breeder," *Journal of Fusion Energy*, **2**, 351 (1982).

17. R. W. MOIR et al, "Fusion Breeder Reactor Design Studies," *Nucl. Technol. Fusion*, **4**, 589 (1983).

18. A. E. DUBBERLEY, K. YOSHIDA, C. E. BOARDMAN, and T. WU, "Super-PRISM Oxide and Metal Fuel Core Designs," Proc. of ICONE 8, Baltimore, MD, USA, April 2-6, 2000.

19. B. VAN DER SHAAF et al., "High Dose, up to 80 DPA, Mechanical Properties of Eurofer 97," *Journal of Nuclear Materials*, **386-388**, 236-240 (2009)

20. A. ALAMO, J. L. BERTIN, V. K. SHAMARDIN, and P. WIDENT, "Mechanical Properties of 9Cr Martensitic Steels and ODS-FeCr Alloys after Neutron Irradiation at 325 ºC up to 42 DPA," *Journal of Nuclear Materials*, **367-370**, 54-59 (2007).

21. A. L. PITNER and R. B. BAKER, "Metal Fuel Test Program in the FFTF," *J. Nucl. Mater.*, **204**, 124 (1993).

22. R. G. PAHL, D. L. PORTER, C. E. LAHM, and G. L. HOFMAN, "Experimental Studies of U-Pu-Zr Fast Reactor Fuel Pins in the Experimental Breeder Reactor-II," *Metall. Trans. A*, **21A**, 1863 (1990).

23. R. G. PAHL, D. L. PORTER, D. C. CRAWFORD, and L. C. WATERS, "Irradiation Behavior of Metallic Fast Reactor Fuels," *Journal of Nuclear Materials,* **188**, 3 (1992).

24. Y. I. CHANG, "Technical Rationale for Metal Fuel in Fast Reactors," *Nuclear Engineering and Technology*, **39**, 161 (2007).

25. G. RIMPAULT et al., "The ERANOS Code and Data-System for Fast Reactor Analyses," *Proc. Int. Conf. New Frontiers of Nuclear Technology: Reactor Physics, Safety and High-Performance Computing (PHYSOR 2002)*, Seoul, Korea, October 7–10, 2002, American Nuclear Society (2002).

26. G. RIMPAULT, D. HONDE, and J.M. RIEUNIER, "ERANOS : MANUEL DES METHODES: Transferts Internes de Données Nucléaires," *ERANOS Documentation*, reference #NT - SPRC - LEPh - 93-252, p. 81. CEA.

27. Private communication with Dr. Ed Hoffman, Argonne National Lab, December 2012.